Strål
säkerhets
myndigheten
Swedish Radiation Safety Authority

Authors: Imre Pázsit
Tran Hoai Nam
Victor Dykin
Anders Jonsson

Research

2013:04

Research and Development Program in Reactor Diagnostics and Monitoring with Neutron Noise Methods, Stage 18

Report number: 2013:04 **ISSN:** 2000-0456
Available at www.stralsakerhetsmyndigheten.se

SSM perspective

Background

This report constitutes Stage 18 of a long-term research and development program concerning the development of diagnostics and monitoring methods for nuclear reactors.

Results up to Stage 17 were reported in SKI and SSM reports, as listed below and in the Summary. The results have also been published in international journals and have been included in both licentiate- and doctor's degrees.

Objectives of the project

The objective of the research program is to contribute to the strategic research goal of competence and research capacity by building up competence within the Department of Nuclear Engineering at Chalmers University of Technology regarding reactor physics, reactor dynamics and noise diagnostics. The purpose is also to contribute to the research goal of giving a basis for SSM's supervision by developing methods for identification and localization of perturbations in reactor cores.

Results

The program executed in Stage 18 consists of the following three parts:

- Application of CoreSim with a two-dimensional model of vibrating fuel assemblies, for the calculation of ex-core detector noise throughout a fuel cycle;
- An investigation of the neutron noise, induced by propagating perturbations, in various thermal and fast reactor systems, in two-group theory;
- A consistent derivation of the point kinetic term of the noise in circulating fuel reactors and an analysis of the of the deviation from traditional system;
- Development of a simulation model to simulate bubbly two-phase flow with axially dependent void fraction and void velocity.

Project information

Responsible at SSM has been Ninos Garis.
SSM references: SSM 2011/2069

Previous SKI reports: 95:14 (1995), 96:50 (1996), 97:31 (1997), 98:25 (1998), 99:33 (1999), 00:28 (2000), 01:27 (2001), 2003:08 (2003), 2003:30 (2003), 2004:57 (2004), 2006:34 (2006), 2008:39 (2008).

Previous SSM reports: 2009:38 (2009), 2010:22 (2010), 2011:29 (2011).

Strål
säkerhets
myndigheten
Swedish Radiation Safety Authority

Authors: Imre Pázsit, Tran Hoai Nam, Victor Dykin and Anders Jonsson
Chalmers University of Technology,
Department of Nuclear Engineering, Göteborg

2013:04

Research and Development Program in Reactor Diagnostics and Monitoring with Neutron Noise Methods, Stage 18

Date: November 2012
Report number: 2013:04 **ISSN:** 2000-0456
Available at www.stralsakerhetsmyndigheten.se

This report concerns a study which has been conducted for the Swedish Radiation Safety Authority, SSM. The conclusions and viewpoints presented in the report are those of the author/authors and do not necessarily coincide with those of the SSM.

SSM 2013:04

Contents

Summary

This report gives an account of the work performed by the Department of Nuclear Engineering, Chalmers University of Technology, in the frame of a research contract with the Swedish Radiation Safety Authority (SSM), contract No. SSM 2011-2069. The present report is based on work performed by Imre Pázsit, Tran Hoai Nam, Victor Dykin and Anders Jonsson, with Imre Pázsit being the project leader.

This report describes the results obtained during Stage 18 of a long-term research and development program concerning the development of diagnostics and monitoring methods for nuclear reactors. The long-term goals are elaborated in more detail in e.g. the Final Reports of Stages 1 and 2 (SKI Report 95:14 and 96:50, Pázsit et al. 1995, 1996). Results up to Stage 17 were reported in (Pázsit et al. 1995, 1996, 1997, 1998, 1999, 2000, 2001, 2003a, 2003b; Demazière et al, 2004; Sunde et al, 2006: Pázsit et al. 2008, 2009, 2010, 2011).

The program executed in Stage 18 consists of four parts as follows:

- Application of CoreSim with a two-dimensional model of vibrating fuel assemblies, for the calculation of ex-core detector noise throughout a fuel cycle;
- An investigation of the neutron noise, induced by propagating perturbations, in various thermal and fast reactor systems, in two-group theory;
- A consistent derivation of the point kinetic term of the noise in circulating fuel reactors and an analysis of the deviation from traditional systems;
- Development of a simulation model to simulate bubbly two-phase flow with axially dependent void fraction and void velocity.

The work performed in each part is summarized below.

1. Application of CoreSim with a two-dimensional model of vibrating fuel assemblies, for the calculation of ex-core detector noise throughout a fuel cycle

In the research project run in collaboration with Ringhals, we found that the amplitude of the peak in the ex-core neutron APSDs, corresponding to the beam mode vibrations of the core barrel, increases during the cycle, but returns to the initial value after refuelling. As described in Stage 17, the reason of this phenomenon is not understood, and the only plausible explanation is that the peak around 8 Hz is given rise by the individual vibrations of one or more fuel assemblies, and that for such vibrations the scaling factor between mechanical vibrations and the induced neutron noise increases with increasing burn-up and decreasing boron content in the coolant.

The validity of this assumption can be investigated by noise calculations, performed by the noise simulator tool Core Sim, developed at the Department (Demazière 2004, 2011). In the previous Stage preparations were made and tested such that Core Sim should be able to handle vibrating fuel assemblies as perturbations. In the present Stage a thorough investigation of the evolution during the cycle of the amplitude of the ex-core neutron noise, induced by fuel assembly vibrations, was performed. It was found

that the noise amplitude can both increase and decrease during the cycle, depending on the position and the vibration patterns of the fuel assembly.

2. An investigation of the neutron noise, induced by propagating perturbations, in various thermal and fast reactor systems, in two-group theory

By using two-group theory, the neutron noise induced by propagating perturbations (propagation noise for short) in both the fast and the thermal group, has been calculated. The purpose is to investigate the dependence of the properties of the space-dependent fast and thermal propagation noise on the static neutron spectrum as well as on the presence of the fluctuations of several cross sections. The motivation for this study arose in connection with recent work on neutron noise in molten salt reactors (MSR) with propagating fuel of various compositions. Some new features of the induced noise were observed, but it was not clear whether these were due to the propagating perturbation alone, or to the propagation of the fuel and hence that of the delayed neutron precursors, which exist only in liquid fuel systems.

Hence the space-dependent propagation noise was investigated in a one-dimensional homogeneous model of various reactor systems. Four different reactor systems with widely varying spectral properties were investigated. The present study serves to clarify the significance of the spectral properties of the different cores through calculating the propagation noise in four different reactor systems, as well as considering the influence of the perturbation of the various cross sections. By comparing the results with those obtained in MSR, the effect of the moving fuel on the propagation noise is clarified. It is shown that in fast systems the noise in the fast group is much larger than in the thermal group and hence can gain diagnostic importance. It is also shown that the co-existence of several cross section fluctuations leads to qualitatively and quantitatively new characteristics of the noise, hence it is important to model the effect of e.g. temperature fluctuations of the coolant in a proper way.

3. A consistent derivation of the point kinetic term of the noise in circulating fuel reactors and an analysis of the deviation from traditional systems

In the theory of neutron noise in power reactors, the validity of the various kinetic approximations has a special significance regarding the possibilities for noise diagnostics. Whether a system behaves in a point kinetic or strongly space dependent manner, determines the possibilities of identifying and locating perturbations in the core, or to determine integral parameters from measurements in a single point.

However, derivation of the point kinetic equations for Molten Salt Reactors (MSR), is not as simple as for traditional reactors, due to the streaming term appearing in the precursor equations. Curiously, the solution for the full problem, i.e. the space- and frequency dependent neutron noise, can be given in a compact analytical form for the case of infinite fuel velocity. From the full solution, the point kinetic component can be calculated analytically by using simple orthogonality relations. This is performed in this work. It is shown that for an MSR the point kinetic component in the frequency domain cannot be factorized into the reactivity and a zero power transfer function; a slightly more complicated expression is obtained and discussed.

4. Development of a simulation model to simulate bubbly two-phase flow with axially dependent void fraction and void velocity

This work concerns the development and application of a method of emulating bubbly flow by generating bubbles with random sampling methods. The randomly generated bubbles are transported by the flow with an axially dependent velocity determined by mass conservation.

The simulation model is constructed such that the arising flow has quantitatively and qualitatively similar properties to those observed in real boiling water reactors (BWRs) what regards the mean axial void fraction and void velocity. The final purpose of the modeling is that by using the simulated random two phase flow as input, one can generate "synthetic" neutron noise signals with a simple neutronic transfer function, on which the possibility of reconstructing the axial void profile from in-core neutron noise measurements can be studied by standard spectral noise analysis methods. The use of the model for simulating the induced neutron noise and investigating the unfolding methods for void fraction determination lies outside the scope of this work. Here only the properties of the flow simulation model are described, and some properties of the generated flow are demonstrated and discussed.

Sammanfattning

Denna rapport redovisar det arbete som utförts inom ramen för ett forskningskontrakt mellan Avdelningen för Nukleär Teknik, Chalmers tekniska högskola, och Strålsäkerhetsmyndigheten (SSM), kontrakt Nr. SSM 2011-2069. Rapporten är baserad på arbetsinsatser av Imre Pázsit, Tran Hoai Nam, Victor Dykin och Anders Jonsson, med Imre Pázsit som projektledare.

Rapporten beskriver de resultat som erhållits i etapp 18 av ett långsiktigt forsknings- och utvecklingsprogram angående utveckling av diagnostik och övervakningsmetoder för kärnkraftsreaktorer. De långsiktiga målen har utarbetats noggrannare i slutrapporterna för etapp 1 och 2 (SKI Rapport 95:14 och 96:50, Pázsit et al. 1995, 1996). Uppnådda resultat till och med etapp 17 har redovisats i referenserna (Pázsit et al, 1995, 1996, 1997, 1998, 1999, 2000, 2001, 2003a, 2003b; Demazière et al, 2004; Sunde et al, 2006; och Pázsit et al, 2008, 2009, 2010, 2011).

Det utförda forskningsarbetet i etapp 18 består av de fyra följande delarna:

- Tillämpning av brussimulatorn CoreSim för att beräkna bruset från vibrerande bränslepatroner i ”ex-core” detektorer;
- Undersökning av neutronbrus som induceras av störningar i termiska och snabba reaktorer med två-grupp teori;
- Härledning av punkt-kinetiska termen av bruset i reaktorer med cirkulerande bränsle och analys av skillnader mot traditionella system;
- Utveckling av modeller för att simulera tvåfasflöde med axiellt beroende voidfraktion och voidhastighet.

Det utförda arbetet i varje del summeras nedan.

1. Tillämpning av brussimulatorn CoreSim för att beräkna bruset från vibrerande bränsleknippen i ”ex-core” detektorer

I forskningsprojektet som utförs i samarbete med Ringhals har vi identifierat att amplituden hos toppen i autospektrum för ex-core detektorerna motsvarande pendelmodvibrationer hos moderatortanken ökar under cykeln, men återvänder till initiala värden efter bränslebyte. Som tidigare beskrivits i etapp 17 är orsaken till detta fenomen inte klarlagt fullt ut, och den enda rimliga förklaringen är att toppen runt 8 Hz uppkommer från individuella vibrationer hos en eller flera bränsleknippen, och att skalfaktorn mellan sådana mekaniska vibrationer och det inducerade neuronbruset ökar med ökad utbränning och minskad borhalt i reaktorkylvattnet.

Giltigheten för detta antagande kan undersökas med brusanalysberäkningar utförda med brussimulatorn CoreSim som utvecklats vid avdelningen (Demazière 2004, 2011). I den tidigare etappen förbereddes och testades CoreSim för att kunna hantera vibrerande bränsleknippen som störningar. I denna etapp har en ingående utredning genomförts avseende utvecklingen av amplituden hos ex-core neutronbruset inducerat av vibrationer hos bränsleknippen under cykeln. Det kunde konstateras att brusamplituden

kan både öka och minska under cykeln beroende på position och vibrationsmönster hos bränsleknippet.

2. Undersökning av neutronbrus som induceras av störningar i termiska och snabba reaktorer med två-grupp teori

Neutronbruset inducerat av störningar (propagerande brus) i både den snabba och termiska gruppen har beräknats genom att använda tvågruppsteori. Syftet är att undersöka hur egenskaperna hos det rumsberoende snabba och termiska propagerande bruset beror av det statiska neutronspektrumet, såsom närvaron av fluktuationer i flera tvärsnitt. Motivet för denna studie uppstod i samband med ett färskt arbete om smältsaltreaktorer (MSR) med cirkulerande bränsle av varierande komposition. Några nya kännetecken för det inducerade bruset observerades, men det var inte tydligt huruvida dessa enkom berodde på den propagerande störningen, eller på cirkulationen av bränslet, och följaktligen de fördröjda neutronföregångarna vilka existerar endast i flytande bränslesystem.

Det rumsberoende propagerande bruset undersöktes i en endimensionell homogen modell av olika reaktorsystem. Fyra olika reaktorsystem med vida varierande spektrala egenskaper undersöktes. Den aktuella studien utgör underlag för att klargöra signifikansen av spektrala egenskaper för de olika härdarna genom att beräkna det propagerande bruset i de fyra olika reaktorsystemen, samtidigt som inflytandet av störningen på olika tvärsnitt behandlas. Genom att jämföra resultaten med dem som erhållits från MSR-studien är effekten av bränslets cirkulation på det propagerande bruset klargjort. Det har visats att bruset i den snabba gruppen är mycket större jämfört med den termiska gruppen i ett snabbt system, och kan därför vinna i betydelse för diagnostiska ändamål. Det demonstreras också att samexistens av flera tvärsnitts-fluktuationer leder till kvalitativt och kvantitativt ny karakteristik hos bruset, och därför är det viktigt att modellera effekten av exempelvis temperaturfluktuationer hos kylmedlet på ett korrekt sätt.

3. Härledning av punkt-kinetiska termen av bruset i reaktorer med cirkulerande bränsle och analys av skillnader mot traditionella system

Giltigheten av olika kinetiska approximationer i teorin om neutronbrus i effektreaktorer har speciell signifikans avseende möjligheterna för brusdiagnostik. Huruvida ett system uppför sig på ett punktkinetiskt eller starkt rumsberoende sätt bestämmer möjligheterna att identifiera och lokalisera störningarna i härden, eller att bestämma globala parametrar från mätning i en enstaka punkt.

Härledning av punktkinetiska ekvationer för smältsaltreaktorer är dock ej så enkla som för traditionella reaktorer beroende på strömningstermen som uppkommer i ekvationen för föregångare. Egendomligt nog kan lösningen för det hela problemet, d.v.s. det rums och frekvensberoende neutronbruset, ges i en kompakt analytisk form för fallet med oändlig bränslehastighet. Den punktkinetiska komponenten kan beräknas analytiskt från helhetslösningen genom att använda enkla ortogonala samband, vilket är utfört i detta arbete. Det visas att den punktkinetiska komponenten i frekvensdomänen för en MSR inte kan faktoriseras i reaktivitets- och nolleffektsöverföringsfunktionen; ett något mer komplicerat uttryck erhålls och diskuteras.

4. Utveckling av modeller för att simulera tvåfasflöde med axiellt beroende voidfraktion och voidhastighet

Detta arbete rör utvecklingen och tillämpningen av en metod för att emulera bubbelflöde genom att generera bubblor med en stickprovsmetod. De slumpmässigt genererade bubblorna transporteras med flödet med en axiellt beroende hastighet som bestäms utifrån massbevarandet.

Simuleringsmodellen är konstruerad så att det uppkomna flödet har kvantitativt och kvalitativt liknande egenskaper som de som observeras i verkliga kokvattenreaktorer avseende medelvärde på axiell voidfraktion och voidhastighet. Det slutgiltiga syftet med modelleringen är att genom att använda simulerat slumpmässigt tvåfasflöde som indata så kan man generera artificiella neutronbrussignaler med en enkel neutronisk överföringsfunktion, vilket möjliggör rekonstruktion av den axiella voidprofilen från in-core neutronbrusmätningar studerade med normala spektralanalysmetoder. Användandet av modellen för att simulera inducerat neutronbrus och undersöka utvikningsmetoder för voidhaltsbestämningar ligger utanför ramarna för detta arbete. Här beskrivs endast egenskaperna hos flödessimuleringsmodellen, och några egenskaper hos det genererade flödet demonstreras och diskuteras.

1 Application of CoreSim with a two-dimensional model of vibrating fuel assemblies, for the calculation of ex-core detector noise throughout a fuel cycle

1.1 Introduction

Calculation of the noise in a power reactor in a realistic model, accounting for inhomogeneous core composition, burnup effects etc., is necessary in many applications. To this order a numerical tool, the so-called noise simulator, was developed in Chalmers University of Technology which can take input for the material composition and geometry of real reactor cores and calculate the induced frequency-dependent noise (Demazière 2004). This tool was first developed to calculate the transfer functions of a reactor in a frequency domain and in 2D Cartesian coordinate, known as the Green's functions, and then, the space- and frequency-dependent neutron noise induced by the fluctuation of macroscopic cross sections as a noise source is calculated using the transfer functions. Thereafter, the tool, named as CORE SIM, was extended to solve also the static neutron fluxes and the neutron noise based on a two-group diffusion theory in 3D Cartesian coordinate. This tool has been used in a number of applications (Demazière 2009, 2011).

One particular application concerns the calculation of the ex-core neutron noise induced by core-barrel vibrations. In the research project done in collaboration with Ringhals, we found that the amplitude of the peak in the ex-core neutron auto-power spectrum densities (APSDs), corresponding to the beam mode vibrations of the core barrel, increases during the cycle, but returns to the initial value after refuelling, at the beginning of the next cycle. The reason for this behaviour is not understood. One guess, expressed by experts is that the scaling factor between core barrel displacement and the normalised neutron noise changes with the change of the boron content and flux redistribution in the core due to burn-up. We have investigated whether such a statement could be confirmed by the use of the noise simulator (Pázsit et al. 2010). However, we did not find any increase of the normalised noise with constant vibration amplitude during the cycle.

In some recent work (Pázsit et al. 2008, 2010), we have arrived at the conclusion that the 8 Hz peak in the ex-core spectra, corresponding to the beam mode, consists of two peaks close to each other in frequency. The two peaks have different origins and different time evolution during the cycle. The peak closer to 7 Hz is induced by the core barrel vibrations, and its amplitude does not change significantly during the cycle. The peak close to 8 Hz is due to the individual fuel assembly vibrations, and its amplitude increases monotonically during the cycle. The fact that vibrations of individual fuel assemblies can contribute to the ex-core noise has been suggested already by Sweeney et al. (1985). These authors also claim that the ex-core noise induced by such vibrations increases during the cycle due to the change of boron concentration and burn-up effects.

The present work aims to investigate the possibility to confirm the validity of this statement using the noise simulator, CORE SIM. Numerical calculations for modeling

fuel assembly vibrations and evaluating the response of ex-core detectors have been performed based on the Ringhals-3 PWR core in cycle 15. Three models of pendular vibrations have been simulated for an individual fuel assembly at 8 Hz and at several different locations in the core. Then, the normalized noise at the four ex-core detectors which are assumed to be located in the outer periphery of the core reflector is evaluated at the beginning, middle and end of cycle in order to investigate the effect of fuel burnup on the ex-core noise.

1.2 Calculation of the neutron noise

The noise simulator, CORE SIM, developed at Chalmers University of Technology is a tool for simulating the space- and frequency dependent noise induced by spatially distributed or localized sources. The tool solves for the noise equation fully in the frequency domain, in which the noise source consists of the stationary fluctuations of the macroscopic cross-sections. The noise equation in the two-group diffusion theory is derived from the time-dependent diffusion equation by splitting the time-dependent parameters into mean values and fluctuations, removing the static equations, performing a Fourier transform, and neglecting the second-order terms (linear theory), and is written as follow (Demazière 2009, 2011):

$$\left[\nabla.\overline{\overline{D}}(\boldsymbol{r})\nabla+\overline{\overline{\Sigma}}_{dyn}(\boldsymbol{r},\omega)\right]\times\begin{bmatrix}\delta\phi_1(\boldsymbol{r},\omega)\\ \delta\phi_2(\boldsymbol{r},\omega)\end{bmatrix}=\begin{bmatrix}S_1(\boldsymbol{r},\omega)\\ S_2(\boldsymbol{r},\omega)\end{bmatrix} \tag{1}$$

The noise source in the r.h.s. of Eq. (1) is calculated from the fluctuations of the cross sections as

$$\begin{bmatrix}S_1(\boldsymbol{r},\omega)\\ S_2(\boldsymbol{r},\omega)\end{bmatrix}=\bar{\phi}_{rem}(\boldsymbol{r})\delta\Sigma_{rem}(\boldsymbol{r})+\overline{\overline{\phi}}_a(\boldsymbol{r})\begin{bmatrix}\delta\Sigma_{a1}(\boldsymbol{r},\omega)\\ \delta\Sigma_{a2}(\boldsymbol{r},\omega)\end{bmatrix}+\overline{\overline{\phi}}_f(\boldsymbol{r})\begin{bmatrix}\delta\nu\Sigma_{f1}(\boldsymbol{r},\omega)\\ \delta\nu\Sigma_{f2}(\boldsymbol{r},\omega)\end{bmatrix}. \tag{2}$$

Here the following notations were used:

$$\overline{\overline{D}}(\boldsymbol{r})=\begin{bmatrix}D_1(\boldsymbol{r}) & 0\\ 0 & D_2(\boldsymbol{r})\end{bmatrix} \tag{3}$$

$$\overline{\overline{\Sigma}}_{dyn}(\boldsymbol{r},\omega)=\begin{bmatrix}-\Sigma_1(\boldsymbol{r},\omega) & \nu\Sigma_{f2}(\boldsymbol{r},\omega)\\ \Sigma_{rem}(\boldsymbol{r}) & -\Sigma_{a2}(\boldsymbol{r},\omega)\end{bmatrix} \tag{4}$$

$$\bar{\phi}_{rem}(\boldsymbol{r})=\begin{bmatrix}\phi_1(\boldsymbol{r})\\ -\phi_1(\boldsymbol{r})\end{bmatrix} \tag{5}$$

$$\overline{\overline{\phi}}_a(\boldsymbol{r})=\begin{bmatrix}\phi_1(\boldsymbol{r}) & 0\\ 0 & \phi_2(\boldsymbol{r})\end{bmatrix} \tag{6}$$

$$\overline{\overline{\phi}}_f(\boldsymbol{r},\omega)=\begin{bmatrix}-\phi_1(\boldsymbol{r}) & -\phi_2(\boldsymbol{r})\\ 0 & 0\end{bmatrix} \tag{7}$$

$$\Sigma_1(\boldsymbol{r},\omega)=\Sigma_{a1}(\boldsymbol{r},\omega)+\Sigma_{rem}(\boldsymbol{r})-\nu\Sigma_{f1}(\boldsymbol{r},\omega) \tag{8}$$

$$\nu\Sigma_{f1,2}(\boldsymbol{r},\omega)=\frac{\nu\Sigma_{f1,2}(\boldsymbol{r})}{k_{eff}}\left(1-\frac{i\omega\beta_{eff}}{i\omega+\lambda}\right) \tag{9}$$

$$\sum_{a1,2}(\boldsymbol{r},\omega)=\sum_{a1,2}(\boldsymbol{r},\omega)+\frac{i\omega}{\upsilon_{1,2}} \tag{10}$$

Equation (1) can be rewritten in a matrix form as

$$\overline{\overline{M}}_{dyn}\times\overline{\delta\phi}=\overline{\delta S} \tag{11}$$

where $\overline{\delta\phi}$ is the neutron noise vector of the fast and thermal groups and $\overline{\delta S}$ represents the noise source vector over the core. The noise source can consist of the fluctuations of the cross-sections as a result of mechanical or thermal processes in the core, such as absorption perturbation, core barrel vibrations, fuel assembly vibrations and so on. In the noise simulator, the noise equation is solved numerically in a matrix form by spatial discretisation based on a finite difference method.

In order to solve the noise equation, the well known Green's function is a powerful technique which allows calculating the space- and frequency dependent noise induced by any noise source when the Green's function is obtained, i.e. the Green function is solved once for all cases for a given system. This technique has been well applied analytically in homogeneous systems and numerically in heterogeneous systems in CORE SIM (Demazière 2009, 2011). The equation for solving the Green's function is similar to the noise equation in (11) but with a Dirac delta function instead of the source on the r.h.s.

$$\overline{\overline{M}}_{dyn}\times\overline{\overline{G}}_{\delta XS}(\boldsymbol{r},\boldsymbol{r}',\omega)=\overline{\delta}_{XS}(\boldsymbol{r}') \tag{12}$$

where, in the two-group theory the Green's matrix has following form

$$\overline{\overline{G}}_{\delta XS}(\boldsymbol{r},\boldsymbol{r}',\omega)=\begin{bmatrix} G_{1\leftarrow1}(\boldsymbol{r},\boldsymbol{r}',\omega) & G_{1\leftarrow2}(\boldsymbol{r},\boldsymbol{r}',\omega) \\ G_{2\leftarrow1}(\boldsymbol{r},\boldsymbol{r}',\omega) & G_{2\leftarrow2}(\boldsymbol{r},\boldsymbol{r}',\omega) \end{bmatrix} \tag{13}$$

where $G_{g\rightarrow g'}(\boldsymbol{r},\boldsymbol{r}',\omega)$ represents the neutron noise at a position $\boldsymbol{r}$ in group g' induced by a Dirac delta perturbation at position $\boldsymbol{r}'$ in group g. In a vector and matrix notation form, the fast and thermal noise can be expressed through the Green's matrix and the noise sources as

$$\overline{\delta\phi}(\boldsymbol{r},\omega)=\int\overline{\overline{G}}_{\delta XS}(\boldsymbol{r},\boldsymbol{r}',\omega)\overline{\delta S}(\boldsymbol{r}',\omega)d\boldsymbol{r}' \tag{14}$$

In case of a point-like vibration in a direction transverse to the considered plane, for example a vibrating control rod, a model of the vibration was suggested by William (1974), in which the fluctuation of cross section of a vibrating rod is expressed through the difference of the Dirac-delta function at the equilibrium and at a displacement as

$$\delta XS(\boldsymbol{r}',t)=\gamma\left\{\delta(\boldsymbol{r}'-\boldsymbol{r}_p-\varepsilon(t))-\delta(\boldsymbol{r}'-\boldsymbol{r}_p)\right\} \tag{15}$$

where γ is the so-called Galanin's constant representing the strength of the perturbation of cross sections, and $\boldsymbol{r}_p$ is the equilibrium position around which the rod vibrates according to the time-dependent displacement function $\boldsymbol{\varepsilon}(t)$. In a two-dimensional vibration, the displacement function is a two component vector, $\boldsymbol{\varepsilon}(t)=\begin{bmatrix}\boldsymbol{\varepsilon}_x(t)\\ \boldsymbol{\varepsilon}_y(t)\end{bmatrix}$, of which the components represent the displacement of the vibrating source around the

equilibrium position in x- and y- directions, respectively. Using the first term in Taylor expansion of the displacement function, and after performing a Fourier transform, one obtains the frequency-dependent fluctuation in Eq. (14) as

$$\delta XS(\boldsymbol{r}',\omega) = -\gamma\varepsilon(\omega)\delta'(\boldsymbol{r}'-\boldsymbol{r}_p) \tag{16}$$

Since the noise source in case of a point-like vibration is written in form of the derivative of the delta function as given in Eq. (16), once the Green's function is obtained, the space-dependent noise can be calculated as follows

$$\overline{\delta\phi}(\boldsymbol{r},\omega) = \gamma\varepsilon(\omega)\cdot\nabla_{r_p}\left[\overline{\overline{G}}_{\delta XS}(\boldsymbol{r},\boldsymbol{r}_p,\omega)\times\bar{\phi}(\boldsymbol{r}_p)\right] \tag{17}$$

where $\bar{\phi}(\boldsymbol{r}_p) = \begin{bmatrix}\phi_1(\boldsymbol{r}_p)\\ \phi_2(\boldsymbol{r}_p)\end{bmatrix}$ represents the static thermal neutron flux at position $\boldsymbol{r}_p$. One can see that using Eq. (17) for noise calculation of a point-like vibrating source requires the calculations of the derivative of the Green's function with respect to the second variable $\boldsymbol{r}_p$, i.e. the equilibrium position of vibrating source.

Another method implemented in CORE SIM could also be used to calculate the ex-core noise through using the adjoint Green's function associated to the forward problem. As pointed out by Pázsit (1992), one of the advantages of the adjoint functions is that if only the neutron noise at a few positions throughout the core but not the space-dependent noise needs to be calculated, the calculation of the derivative of the Green's function with respect to the second variable could be avoided by using a proper adjoint function. The adjoint neutron noise is calculated by

$$\overline{\delta\phi}^{\dagger}(\boldsymbol{r},\omega) = \gamma\varepsilon(\omega)\cdot\nabla_{r_p}\left[\overline{\overline{G}}^{\dagger}_{\delta_{XS}}(\boldsymbol{r}_p,\boldsymbol{r},\omega)\times\bar{\phi}^{\dagger}(\boldsymbol{r}_p)\right] \tag{18}$$

For example, if the noise source is defined as $\delta S_1(\boldsymbol{r},\omega)=0$ and $\delta S_2(\boldsymbol{r},\omega)=\delta(r-r_p)$, and the adjoint noise source is $\delta S_1(\boldsymbol{r},\omega)=0$ and $\delta S_2(\boldsymbol{r},\omega)=\delta(r-r_p)$, then one obtains

$$G^{\dagger}_{2\leftarrow 2}(\boldsymbol{r},\boldsymbol{r}_p,\omega) = G_{2\leftarrow 2}(\boldsymbol{r},\boldsymbol{r}_p,\omega) \tag{19}$$

Since the derivative of the adjoint Green's function in Eq. (18) is taken with respect to the first variable, while it is taken with respect to the second variable in the forward approach. The explanation lies with the fact that the full space-dependence of $G_{g\leftarrow g'}(\boldsymbol{r},\boldsymbol{r}_p,\omega)$ with respect to the first variable is directly obtained from the numerical tool, whereas the full space-dependence of $G_{g\leftarrow g'}(\boldsymbol{r},\boldsymbol{r}_p,\omega)$ with respect to the second variable can only be estimated by performing with many noise source positions, $\boldsymbol{r}_p$. Therefore, using the adjoint functions make it possible to calculate the noise at the ex-core detectors when a proper adjoint source is chosen.

However, in case of a vibrating source with a finite width, e.g vibrating fuel assembly, the induced noise is calculated in the forward approach by taking integral of the both sides of Eq. (17) over the width of the source, then the derivative of Green's function will be eliminated as follows:

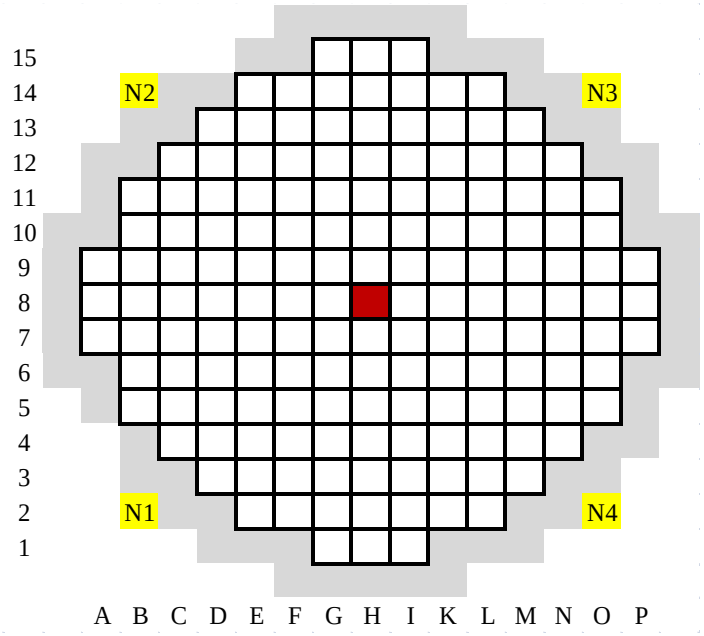

Fig. 1 Configuration of the Ringhals-3 PWR

$$\overline{\delta\phi}(\boldsymbol{r},\omega) = \gamma\varepsilon(\omega)\cdot\int \nabla_{r'}\left[\overline{\overline{G}}_{\delta XS}(\boldsymbol{r},\boldsymbol{r}',\omega)\times\bar{\phi}(\boldsymbol{r}')\right]d\boldsymbol{r}' \qquad (20)$$

In recent development of CORE SIM, a power iteration solution has been implemented to solve for both the static and dynamic equations. In the dynamic problem, the space-dependent noise is calculated for a given noise source at a given frequency. This development would help to avoid problems related to memory requirements in solving the Green's function.

In this work, the noise simulator is used to simulate the pendular vibrations of fuel assemblies and estimate the effect of burnup on the normalized ex-core noise in a 2-D model by assuming that the vibration is perpendicular to the axial direction and the vibrating assembly always remains parallel to itself. Since the solution of Green's function in a 2D model is much simpler than in a 3D model which is usually demanding what regards computation time and memory, the forward Green's function technique will be used to calculate the noise induced by a vibrating fuel assembly.

1.3 Modelling of fuel vibrations

1.3.1 Cross section preparation

Numerical calculations have been performed based on the Ringhals-3 PWR core at cycle 15 using the neutron noise simulator, CORE SIM. The core configuration with four ex-core detectors assumed to be located at the outer periphery of the reflector is illustrated in Fig. 1.

Numerical calculations of the ex-core noise induced by the pendular vibrations of fuel assemblies are performed in a 2-D two-group model, therefore the group constants and kinetic parameters for a 2-D model are required. CORE SIM is developed in coupling with the SIMULATE-3 code to use the cross sections and the kinetic parameters

generated by SIMULATE-3 for dynamic calculations. SIMULATE-3, which is developed based on a polynomial nodal method, provides a two-group cross section set in a 3-D model. In order to use this data in 2-D dynamic calculations, the 3-D cross section set has to be first collapsed to a 2-D data set using the static fluxes as a weighting function. Therefore, the static 3-D calculations were performed using CORE SIM to obtain the keff and static fluxes. Then, the 3-D cross-section set provided by SIMULATE-3 was homogenized to a 2-D model using the static fluxes as weighting functions as following

$$XS_{g,I,J} = \frac{\sum_{K} XS_{g,I,J,K}\phi_{g,I,J,K}V_{I,J,K}}{\sum_{K}\phi_{g,I,J,K}V_{I,J,K}} \tag{21}$$

where, $XS_{g,I,J}$ stands for either the diffusion coefficient, or any of the absorption, scattering or production cross sections in group g. The subscripts I,J,K are the coordinates of the node with $V_{I,J,K}$ representing the volume of the node. In order to preserve the axial leakage in the 3-D core, one has to take the axial leakage into account via a modification of the absorption cross-section in each group as

$$\Sigma^{*}_{a,g,I,J,K} = \Sigma_{a,g,I,J,K} + \frac{L_{g,I,J,K}}{\phi_{g,I,J,K}} \tag{22}$$

where, $L_{g,I,J,K}$ is the axial leakage rate in each node is the 3-D model obtained from static calculation using CORE SIM. The modified absorption cross section is then continuously homogenized to 2-D model as expressed in Eq. (21).

1.3.2 Modeling of fuel vibrations

In the numerical simulation of vibrations, the forward Green's function was used, by having the perturbation (fluctuations in the cross sections) as the inhomogeneous part of the equation. Since the inhomogeneous part in the equation could not be defined as a Dirac delta function, rather as a step-function over one mesh, i.e. the displacement of a fuel assembly is equal to the mesh size which the noise simulator can define. In other words, any vibration could only be defined with a spatial resolution not smaller than the mesh size. However, in a 2-D model, the mesh size of about 2.0-2.5 cm is used which is still too large compared to the displacement of a realistic vibration, where the maximum displacement of vibrating assembly is assumed to be less than 1.0 mm.

One possibility is to use a finer mesh, and calculate the Green's function by moving the inhomogeneous part of the equation with one mesh. If the mesh size is chosen as small as the vibration, the total number of meshes will increase amplitude excessively and may lead to a problem of memory and calculation time. In order to simulate the vibration with a flexible small displacement while avoiding a large number of meshes, the spatial discretization has been reconstructed for the vibrating assembly by adding a very fine mesh around its border while keeping the same mesh size for all other assemblies. Such a method can be applied in 2-D simulation, where a very small displacement of vibration can be simulated while the total number of meshes does not increase much, and therefore does not lead to excessive memory problems and running times. However, by this method, the Green's function which corresponds to the noise

calculation induced by the vibration is fixed to be able to treat only a given assembly but not others.

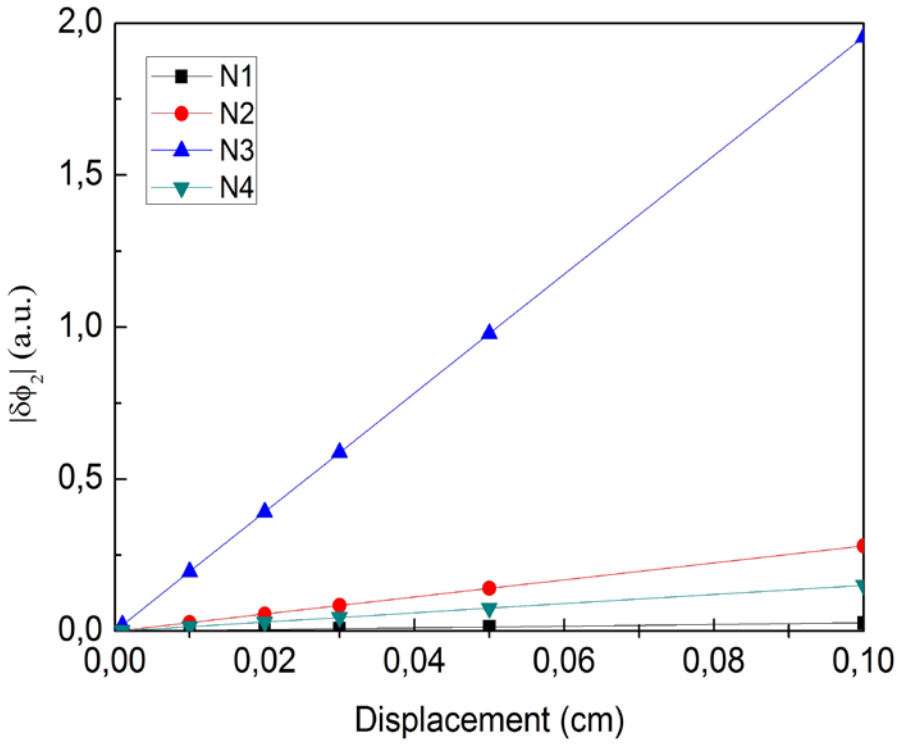

Fig. 2 Ex-core noise vs. vibration strength of assembly M10 (Model 1, f=8 Hz)

First, the static diffusion equations are solved for the k_{eff} and the static fluxes which are later used for determining the noise source and the frequency-dependent cross sections in the noise equation. Then, dynamic calculations are performed to obtain the noise. The fuel assembly vibration is modeled by shifting materials for a very fine mesh around its equilibrium location. It means that we consider the fluctuations in all types of cross-sections.

Fig. 2 shows the dependence of the magnitude of thermal noise of the fuel assembly M10 in y-direction on the vibration amplitude at the four ex-core detectors when the displacement increases from 0.01 to 1.0 mm. One can see that the magnitude of the induced noise increases linearly with the increase of the vibration amplitude. Therefore, a scaling factor can be defined as the ratio of the normalized thermal noise and the displacement of the fuel assembly. In case of an anisotropic vibration, i.e. the vibration in both x- and y-directions, the maximum displacements of the vibration in the directions are described by the amplitude of the displacement functions $\varepsilon_x(\omega)$ and $\varepsilon_y(\omega)$, respectively. Then, the total normalized thermal noise is calculated as a linear combination of the noise induced by the vibration in x- and y- directions as

$$APSD_{\delta\phi_2/\phi_2} = |A_x|^2 \, APSD_x(\omega) + |A_y|^2 \, APSD_y(\omega) \qquad (23)$$

where A_x and A_y are the complex frequency dependent transfer functions between the neutron noise and the fuel assembly vibration in x- or y- direction, respectively, as

Table 1 Data of the Ringhals-3 PWR in cycle 15

Burnup steps	k_{eff}	β_{eff} (pcm)	λ (ms)	υ_1 (cm/s)	υ_2 (cm/s)
BOC	1.00103	596.7	0.084356	1.78631e+07	4.17195e+05
MOC	1.00170	551.1	0.087121	1.81783e+07	4.13994e+05
EOC	1.00062	520.2	0.089139	1.81658e+07	4.04119e+05

calculated by CORE SIM. Their amplitudes $|A_x|$ and $|A_y|$ refer to the scaling factors of the ex-core noise with the vibrations into the respective directions.
Since the isotropic vibration can be expressed through the independent displacement functions, $\varepsilon_x(\omega)$ and $\varepsilon_y(\omega)$, the total noise will be a linear combination of the two components in two directions as given in (23). Therefore, investigating the change of the APSD of the ex-core detector noise throughout the cycle can be done by the APSD or the scaling factors of the ex-core noise throughout the cycle.

1.4 Results obtained with Ringhals-3 PWR

Numerical calculations have been performed for the Ringhals-3 PWR core to investigate the ex-core detector noise throughout the cycle. For this purpose, the calculations were performed at three burnup steps with the parameters of the core as given in Table 1. The noise calculations were performed for the vibration of the fuel assembly at a frequency of 8 Hz. Using the noise simulator, CORE SIM, it is allowed to simulated only the pendular vibration of assemblies in a specific trajectory. Fig. 3 shows examples of three models of the trajectory vibrations.

Figs. 4 - 6 show the static fluxes in the fast and thermal groups at the three burnup steps (BOC, MOC and EOC), at which the fuel assembly vibrations were investigated. Figs. 7 - 9 show the space-dependent amplitude and the phase of the neutron noise induced by the vibrations of a fuel assembly corresponding to the three vibration models, where in Models 2 and 3, the same displacements in x and y directions are assumed. One can see that the in-core fuel vibration indeed affects the noise at ex-core detector noise.

According to Eq. (23), one needs to calculate only the transfer functions A_x and A_y, whose amplitudes yield the scaling factors of the ex-core noise of an assembly in the x and y directions. The effect of any anisotropic vibration can be calculated from these.

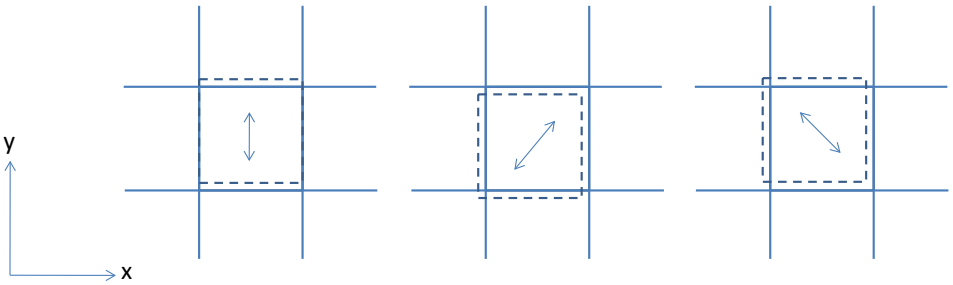

Fig. 3 Three models of pendular fuel assembly vibrations

Calculations of the ex-core scaling factors (amplitudes) and phases have been performed for several assembly locations in the core and are given in Tables 2 - 8. These show the amplitudes (scaling factors) and the phases of the noise at the four ex-core detectors induced by the vibrations of several fuel assemblies in the core. The numerical calculations have been performed at three burnup steps corresponding to the BOC, MOC and EOC. The frequency of vibration is investigated at 8 Hz for all cases. In the measurements, it is found that the APSD or the scaling factors of the ex-core noise always increases throughout the cycle and it is assumed by the hypothesis that the increase of the APSD is due to fuel assembly vibrations. However, according to our results, both increasing and decreasing trends of the scaling factors with cycle burnup are found. Furthermore, the increasing and decreasing intension are not constantly monotonic throughout the cycle. The results show that in case of the assembly at location I9, the scaling factors of the four ex-core detectors decrease monotonically with burnup from BOC to MOC and EOC. On the other hand, in case of the vibrations of assemblies M10, K10, K12 and L13, it is found that the scaling factors of some detectors increase or decrease with burnup, but not monotonically. For example, in the y-directional vibration of M10 assembly, the scaling factor of detector N1 decreases from BOC to MOC and then increases from MOC to EOC, while that of N3 increases from BOC to MOC and then slightly decreases from MOC to EOC. It means that the variation of the scaling factor is not monotonic throughout the burnup cycle.

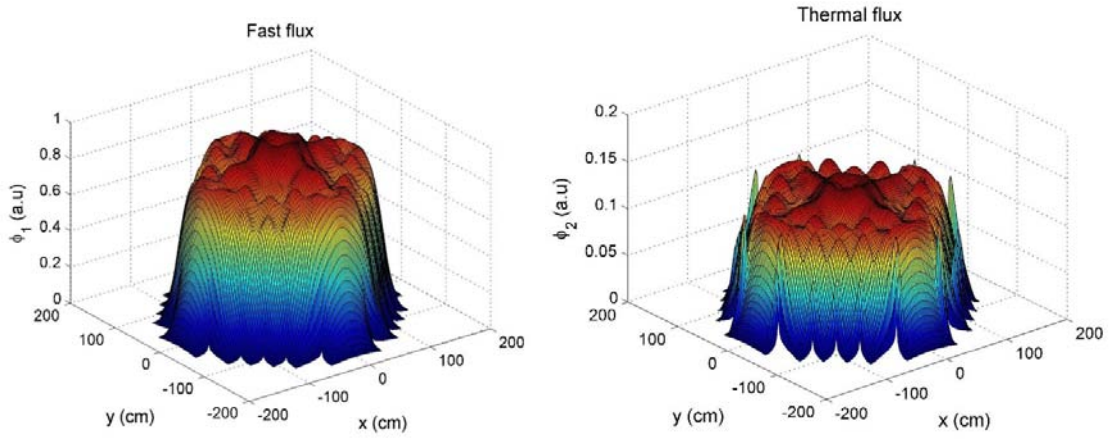

Fig. 4 Static fast (left) and thermal (right) fluxes of the Ringhals-3 PWR at BOC.

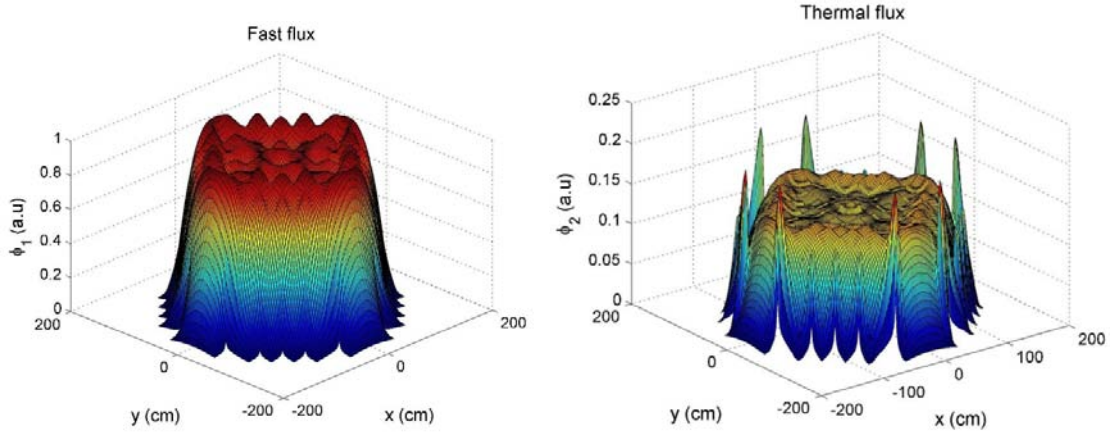

Fig. 5 Static fast (left) and thermal (right) fluxes of the Ringhals-3 PWR at MOC.

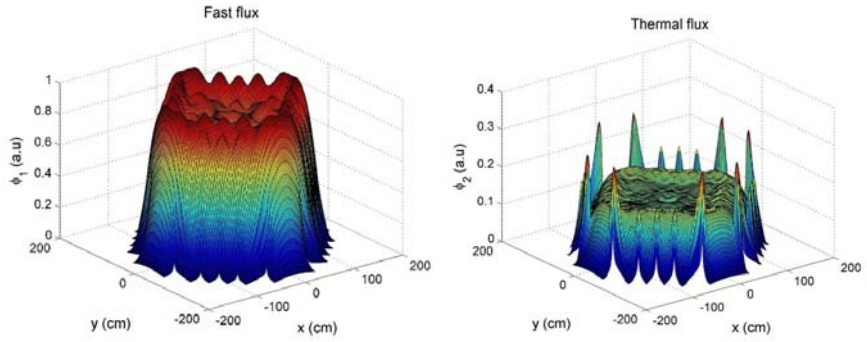

Fig. 6 Static fast (left) and thermal (right) fluxes of the Ringhals-3 PWR at EOC.

To understand more about the properties of ex-core noise, the two cases of assemblies I9 and K11 are selected for further discussions. Figs. 10 and 11 show the fast and thermal fluxes across the I9 and K11 assemblies in x- and y- directions through the cycle. Figs. 12 and 13 shows the cross sections of the two assemblies with burnup. The responses of the four ex-core detectors (N1-N4) with the vibration of the two assemblies are demonstrated in Figs. 14 and 15. From the ex-core noise calculation results for the Ringhals-3 using CORE SIM, it turns out that the numerical results could not agree with the hypothesis that the APSD of the ex-core detector noise induced by fuel assembly vibration increases monotonically throughout the cycle because of the burnup effect, change of boron concentration, etc. The results show that the increase of the APSD of ex-core noise during burnup could be a result of fuel assembly vibrations in some cases but this could not be the only reason of the constant increase as obtained in measurement.

1.5 Conclusions

Ex-core noise calculations have been performed for the Ringhals-3 PWR using the noise simulator, CORE SIM, to investigate the effect of cycle burnup on the scaling factor between the amplitude of the vibrations of fuel assemblies and the induced ex-core neutron noise. The objective was to check a hypothesis by Sweeney et al., according to which the increase of the amplitude of the ex-core noise during the cycle is that the ex-core noise is largely due to the individual vibrations of fuel assemblies, and that the scaling factor between those vibrations and the induced noise increases with burn-up and change of boron concentration.. The results obtained for the Ringhals-3 showed the obvious effect of in-core fuel vibration on the ex-core noise, however no monotonic variation of the APSD with the burn-up was found. The conclusion is that the calculation results did not unambiguously support the hypothesis. The results show that the increase of the APSD of ex-core noise during burnup could be a result of fuel assembly vibrations in some cases, but this could not be the only reason of the constant increase as obtained systematically in measurements.

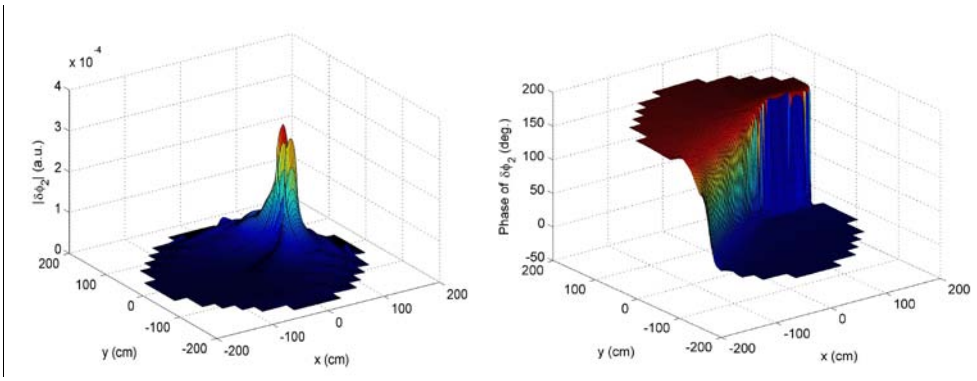

Fig. 7 Magnitude and phase of thermal neutron noise induced by the vibration of fuel assembly M10 at BOC (Model 1, f= 8 Hz).

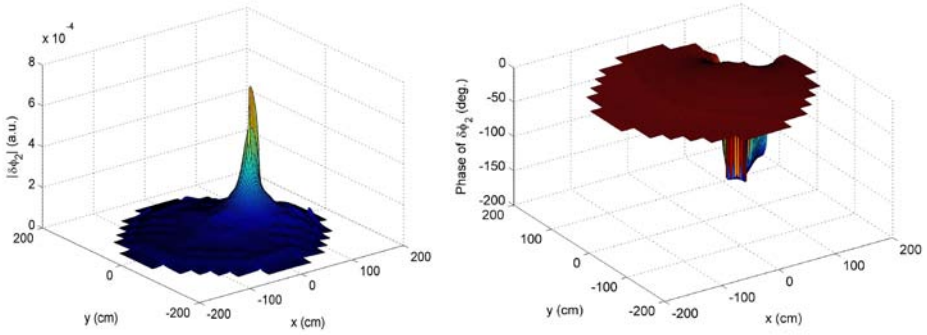

Fig. 8 Magnitude and phase of thermal neutron noise induced by the vibration of fuel assembly M10 at BOC (Model 2, f= 8 Hz).

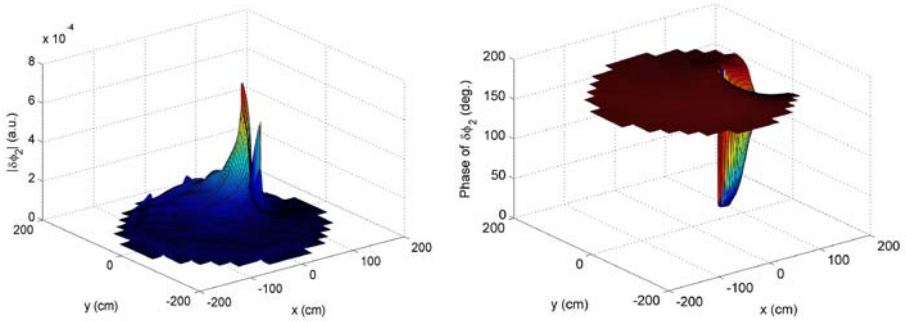

Fig. 9 Magnitude and phase of thermal neutron noise induced by the vibration of fuel assembly M10 at BOC (Model 3, f= 8 Hz).

Table 2 Ex-core noise induced by the vibration of assembly M10 at 8.0 Hz

Ex-core detectors	Burnup steps	X-direction		Y-direction	
		Amplitude	Phase	Amplitude	Phase
N1	BOC	2.161e-4	-0.262	1.794e-5	-0.081
	MOC	2.155e-4	-0.307	1.453e-5	2.466
	EOC	1.772e-4	-0.362	2.697e-5	2.535
N2	BOC	3.266e-4	-0.209	1.417e-4	-0.067
	MOC	3.000e-4	-0.256	9.676e-5	0.025
	EOC	2.331e-4	-0.313	6.764e-5	0.148
N3	BOC	8.157e-4	-0.116	8.765e-4	3.113
	MOC	7.648e-4	-0.142	1.022e-3	3.094
	EOC	6.184e-4	-0.172	1.017e-3	3.076
N4	BOC	3.211e-4	-0.213	6.295e-5	3.008
	MOC	3.384e-4	-0.242	1.234e-4	2.941
	EOC	2.906e-4	-0.282	1.400e-4	2.889

Table 3 Ex-core noise induced by the vibration of assembly I9 at 8.0 Hz

Ex-core detectors	Burnup steps	X-direction		Y-direction	
		Amplitude	Phase	Amplitude	Phase
N1	BOC	6.257e-4	2.907	5.420e-4	2.905
	MOC	4.357e-4	2.866	3.782e-4	2.863
	EOC	3.554e-4	2.815	3.080e-4	2.811
N2	BOC	8.568e-4	2.945	6.727e-4	2.932
	MOC	6.053e-4	2.913	4.760e-4	2.897
	EOC	4.998e-4	2.871	3.920e-4	2.852
N3	BOC	1.187e-3	2.981	1.067e-3	2.983
	MOC	8.586e-4	2.957	7.731e-4	2.959
	EOC	7.168e-4	2.924	6.452e-4	2.927
N4	BOC	7.816e-4	2.935	7.653e-4	2.947
	MOC	5.529e-4	2.900	5.431e-4	2.915
	EOC	4.560e-4	2.856	4.482e-4	2.873

Table 4 Ex-core noise induced by the vibration of assembly H12 at 8.0 Hz

Ex-core detectors	Burnup steps	X-direction		Y-direction	
		Amplitude	Phase	Amplitude	Phase
N1	BOC	5.343e-5	-0.191	5.065e-4	2.869
	MOC	4.607e-5	-0.214	4.659e-4	2.824
	EOC	4.261e-5	-0.255	4.211e-4	2.763
N2	BOC	4.034e-6	-2.206	5.087e-4	2.870
	MOC	7.657e-6	-2.864	4.657e-4	2.824
	EOC	7.891e-6	-2.884	4.205e-4	2.763
N3	BOC	1.778e-4	3.131	1.544e-3	2.997
	MOC	1.487e-4	3.123	1.342e-3	2.968
	EOC	1.328e-4	3.118	1.231e-3	2.935
N4	BOC	3.102e-4	-0.071	1.524e-3	2.996
	MOC	2.489e-4	-0.083	1.346e-3	2.969
	EOC	2.250e-4	-0.101	1.236e-3	2.936

Table 5 Ex-core noise induced by the vibration of assembly L13 at 8.0 Hz

Ex-core detectors	Burnup steps	X-direction		Y-direction	
		Amplitude	Phase	Amplitude	Phase
N1	BOC	1.392e-4	-0.285	2.022e-4	-0.287
	MOC	1.294e-4	-0.332	2.078e-4	-0.337
	EOC	1.144e-4	-0.394	1.849e-4	-0.401
N2	BOC	1.419e-4	-0.286	3.249e-4	-0.225
	MOC	1.266e-4	-0.340	3.378e-4	-0.261
	EOC	1.053e-4	-0.418	3.125e-4	-0.306
N3	BOC	3.480e-4	-3.052	9.357e-4	-0.065
	MOC	3.132e-4	-3.041	8.176e-4	-0.084
	EOC	3.176e-4	-3.040	7.316e-4	-0.103
N4	BOC	1.816e-4	-0.167	1.696e-4	-0.213
	MOC	1.710e-4	-0.193	1.724e-4	-0.252
	EOC	1.606e-4	-0.226	1.531e-4	-0.303

Table 6 Ex-core noise induced by the vibration of assembly K10 at 8.0 Hz

Ex-core detectors	Burnup steps	X-direction		Y-direction	
		Amplitude	Phase	Amplitude	Phase
N1	BOC	1.394e-4	2.855	2.236e-4	2.865
	MOC	1.487e-4	2.794	2.271e-4	2.809
	EOC	1.371e-4	2.730	1.979e-4	2.744
N2	BOC	3.020e-4	2.953	3.094e-4	2.908
	MOC	3.368e-4	2.920	3.127e-4	2.859
	EOC	3.111e-4	2.877	2.777e-4	2.806
N3	BOC	7.864e-4	3.042	1.059e-3	3.035
	MOC	8.654e-4	3.023	1.118e-3	3.016
	EOC	7.918e-4	2.998	9.920e-4	2.991
N4	BOC	1.810e-4	2.888	4.259e-4	2.947
	MOC	1.927e-4	2.833	4.556e-4	2.914
	EOC	1.832e-4	2.781	4.045e-4	2.872

Table 7 Ex-core noise induced by the vibration of assembly K11 at 8.0 Hz

Ex-core detectors	Burnup steps	X-direction		Y-direction	
		Amplitude	Phase	Amplitude	Phase
N1	BOC	2.056e-4	-0.297	1.559e-4	-0.313
	MOC	3.869e-4	-0.337	1.956e-4	-0.362
	EOC	3.841e-4	-0.401	2.173e-4	-0.423
N2	BOC	4.043e-4	-0.207	1.753e-4	-0.304
	MOC	6.765e-4	-0.250	2.247e-4	-0.345
	EOC	6.756e-4	-0.297	2.642e-4	-0.389
N3	BOC	1.674e-3	-0.081	1.300e-3	-0.086
	MOC	2.345e-3	-0.109	1.412e-3	-0.107
	EOC	2.300e-3	-0.134	1.456e-3	-0.133
N4	BOC	2.980e-4	-0.251	4.507e-4	-0.177
	MOC	6.178e-4	-0.265	5.383e-4	-0.209
	EOC	6.324e-4	-0.310	5.718e-4	-0.252

Table 8 Ex-core noise induced by the vibration of assembly K12 at 8.0 Hz

Ex-core detectors	Burnup steps	X-direction		Y-direction	
		Amplitude	Phase	Amplitude	Phase
N1	BOC	1.990e-5	-0.103	2.136e-4	-0.261
	MOC	1.076e-5	2.341	2.146e-4	-0.306
	EOC	2.299e-5	2.499	1.754e-4	-0.361
N2	BOC	6.054e-5	3.014	3.199e-4	-0.212
	MOC	1.181e-4	2.945	3.379e-4	-0.242
	EOC	1.348e-4	2.893	2.886e-4	-0.281
N3	BOC	8.685e-4	3.115	7.858e-4	-0.117
	MOC	1.000e-3	3.095	7.523e-4	-0.143
	EOC	9.967e-4	3.078	6.016e-4	-0.173
N4	BOC	1.443e-4	-0.071	3.184e-4	-0.209
	MOC	1.048e-4	0.005	2.967e-4	-0.257
	EOC	7.562e-5	0.101	2.279e-4	-0.314

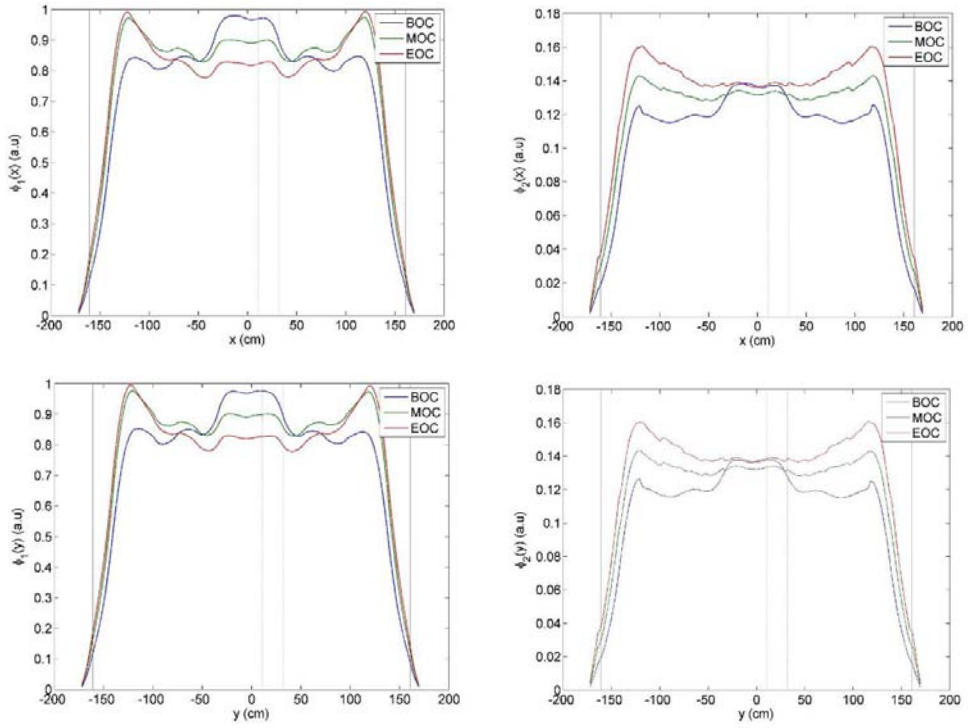

Fig. 10 Neutron fluxes across the vibrating assembly I9. The dotted vertical lines show the position of assembly I9 in the core.

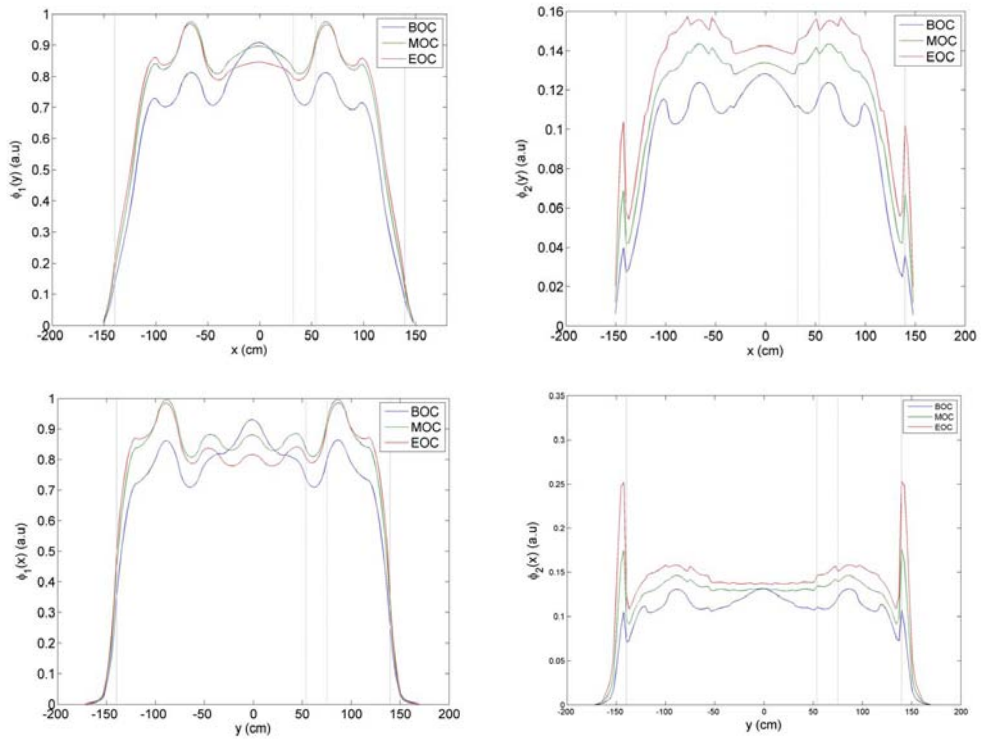

Fig. 11 Neutron fluxes across the vibrating assembly K11. The dotted vertical lines show the position of assembly K11 in the core.

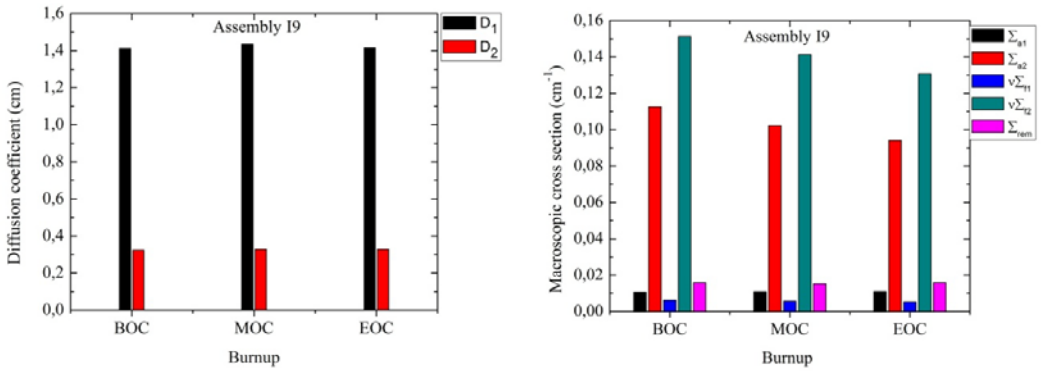

Fig. 12 *Macroscopic cross sections of assembly I9 during burnup.*

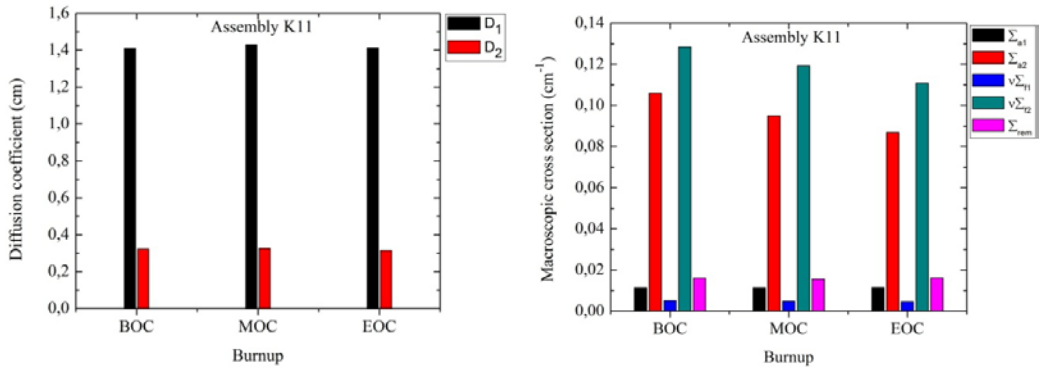

Fig. 13 Macroscopic cross sections of assembly K11 during burnup.

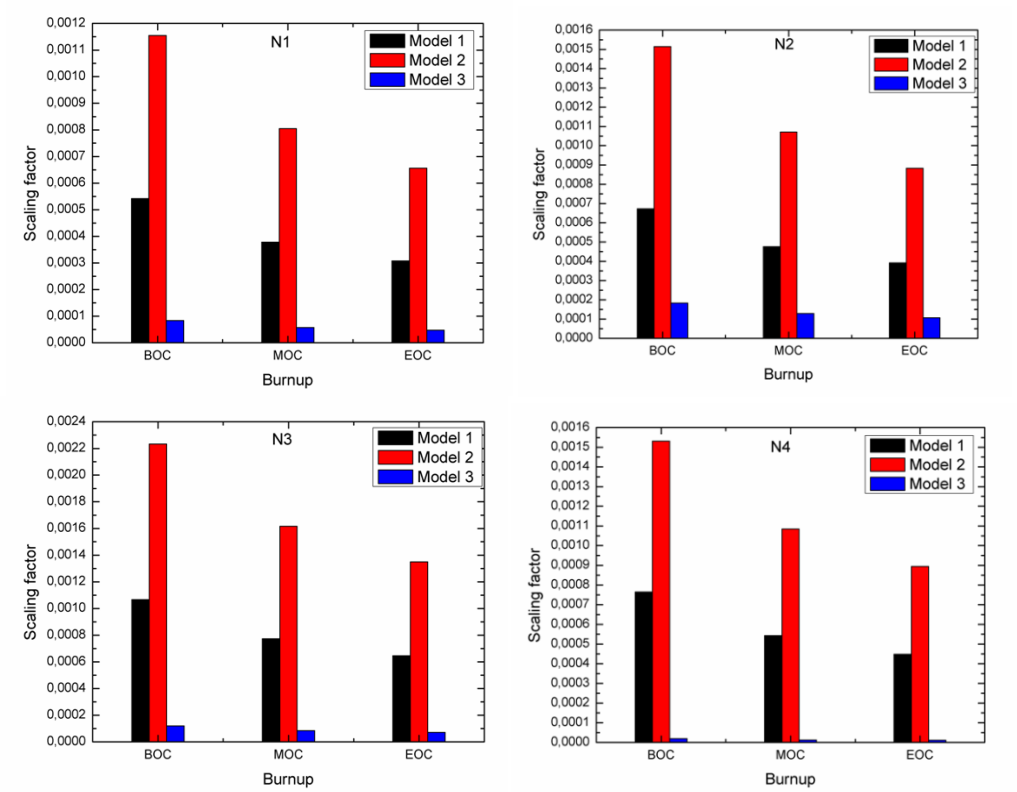

Fig. 14 Scaling factors of ex-core noises induced by the vibration of assembly I9 of the Ringhals-3 PWR at 8 Hz.

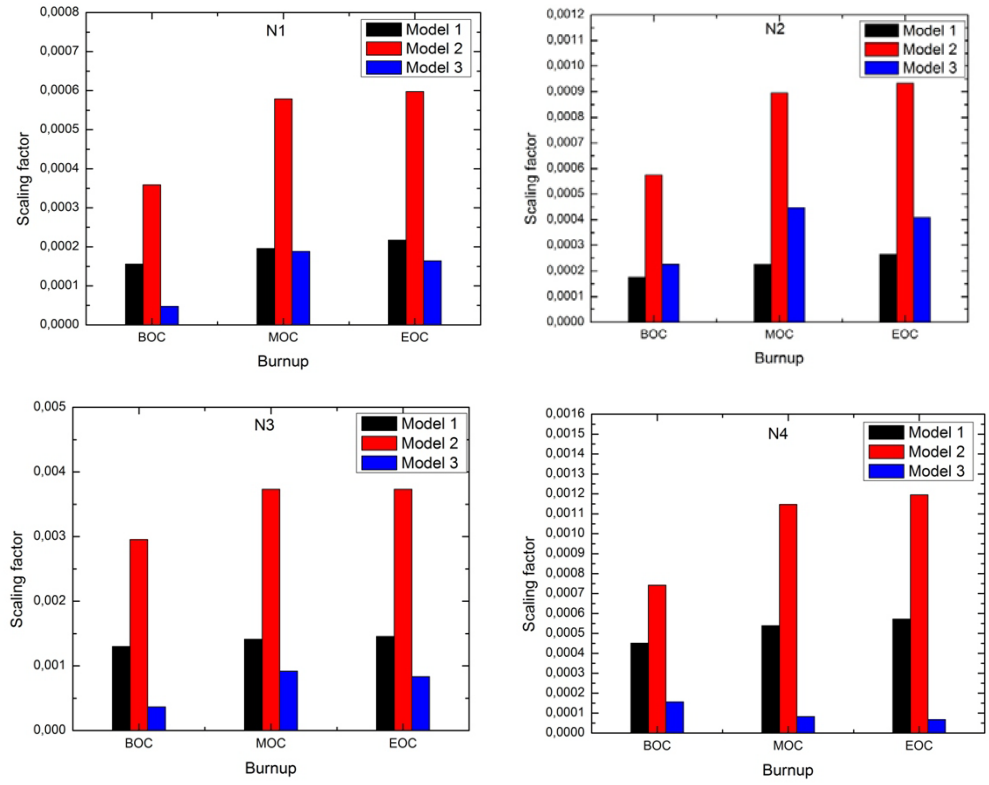

Fig. 15 Scaling factors of ex-core noises induced by the vibration of assembly K11 of the Ringhals-3 PWR at 8 Hz.

2 An investigation of the neutron noise, induced by propagating perturbations, in various thermal and fast reactor systems, in two-group theory

2.1 Introduction

The space-dependent behaviour of the neutron noise in power reactors was investigated intensively in a variety of papers for the last 40 years (for reviews, see Williams (1974); Kosály (1980); Pázsit and Demazière (2011)). Somewhat remarkably, however, as noted recently (Pázsit and Dykin (2010)), the in-core noise in PWRs and BWRs, induced by propagating perturbations (inlet temperature fluctuations and two-phase flow, respectively), has remained an exception. The reasons for this are also discussed in (Pázsit and Dykin (2010)). The space dependence here refers to the axial dependence of the induced noise, i.e. its space dependence in the same direction as the flow/propagation itself. The radial dependence of the neutron noise induced by a local (channel-type) instability was investigated in the past; however, in this case, the axial structure and hence the propagating character of the noise source does not play a role.

The space dependence of the neutron noise induced by propagating perturbations (for which we suggest to introduce the shorthand notation “propagation noise” as will also be used in this report) received interest recently due to investigations of the neutron noise in molten salt reactors (MSR). In such reactors the circulation of the fuel is likely to induce propagating perturbations due to inhomogeneities in the density/temperature, fuel concentration in the salt, locally slightly varying burnup in the fuel etc. The propagation noise induced by such perturbations was investigated in some recent publications (Pázsit and Jonsson, 2010; Jonsson and Pázsit, (2011).

In the second of the above references the neutron noise was calculated in a two-group approach, in three different systems with different material properties which lead to different neutron spectra. The motivation came from the fact that the MSR, being one of the six selected Gen-IV systems, can be built either with a fast or with a thermal spectrum, dependent on the moderator and the fuel used. Hence three different systems were selected, one with a very soft thermal spectrum, representing a graphite moderated thorium fuelled MSR, a Gen-II light water reactor (BWR) and a high conversion fast system operating with MOX fuel, with fast spectrum. Even these two latter systems were assumed to contain moving fuel in liquid form, representing models of possible MSRs, only the group constants were taken from the corresponding traditional systems. By selecting these three systems, the significance of the spectral properties of the core on the spatial and frequency properties of the induced propagation noise, including the relative significance of the local component of the noise, could be investigated.

The above mentioned investigation was the first of its kind because, with a very few exceptions (such as Yoshioka et al., 1998) the spectral properties of the neutron noise, and the significance of the spectral properties of the core on the characteristics of the neutron noise have not been investigated before. All quantitative studies were made in thermal LWRs, and only the influence of the system size and the frequency on the

thermal neutron noise was of interest. The investigation of the characteristics of the noise in systems with different spectral properties yielded some new features and tendencies regarding the induced noise. However, it was a somewhat unfortunate circumstance that these novel studies were not performed in traditional systems with stationary fuel, rather directly on MSR-type systems with moving fuel, i.e. with moving delayed neutron precursors. Hence it was not possible to say whether these new properties were due to the effect of the propagating perturbations and/or the spectral properties alone, or to the propagation of the fuel and hence that of the delayed neutron precursors. In other words, it was not clear if the same properties would be observed in traditional systems with stationary fuel.

We decided therefore to make a thorough investigation of the noise properties in various traditional systems (i.e. with stationary fuel) with widely differing spectral properties. Four different systems were selected:

- a fast reactor with MOX fuel
- a BWR
- a PWR
- a heavy water core (representing a CANDU).

By selecting these four different systems, a wider range of spectral properties could be covered. This way the present study can also be considered as the first attempt to investigate the applicability of noise analysis to systems significantly different from the LWR cores dominating in quantitative studies of noise diagnostics so far, as well as the first attempt to study the spectral properties of the induced neutron noise in a two-group model. The present study also serves to clarify the significance of the core properties and that of the fuel propagation, through calculating the propagation noise in cores with static fuel in the four different reactor systems ranging from Gen-II to GEN-IV characteristics and comparing it with the results obtained in the MSR study of Jonsson and Pázsit (2011). One result of these investigations is that in fast systems the neutron noise in the fast group has a much larger amplitude than that of the thermal noise, and hence it can be utilised in fast system for diagnostic purposes.

Another novelty of the present investigations is the modelling of the noise source. In the past studies of the propagation noise, the perturbation was modelled by the fluctuations of one single macroscopic cross section: either the thermal absorption cross section (in case of inlet coolant temperature fluctuations in PWRs), or the removal cross section (for the void fluctuations in BWRs). This is because it was considered that the main features of the problem can be described sufficiently well by considering the fluctuations of a “dominating” cross section. The validity of this assumption is investigated in this paper by considering the noise source as temperature fluctuations of the coolant and calculating the relative weight of the fluctuations of all cross sections. It turned out that the effect of the aggregate of the cross section fluctuations has qualitatively and quantitatively different properties than in the case of a single cross section fluctuation. This underlines the need of proper modelling of noise sources at least for calculating the neutron noise induced by propagating temperature and density fluctuations.

2.2 Basic considerations

The investigation of the neutron noise induced by various perturbations is usually performed through the Green's function method. This has the practical advantage that it is more straightforward to obtain analytical results, as well as that the Green's function itself, representing the dynamic transfer function of the system, gives insight into the properties of the system which are not dependent on the perturbation. Hence in the final result it is easier to identify if a certain feature can be attributed to the system properties or to the perturbation.

In a two-group approach, there is an alternative possibility due to the fact that the two-group equations are not self-adjoint. Hence, as it was suggested by van Dam (1975, 1976) one can use the dynamic adjoint function instead of the Green's function (Pázsit and Demazière (2011)). Actually, due to some differences between the direct and the adjoint Green's function, in most works the dynamic adjoint was used. One reason is that in the two-group case, where both the noise source and the induced neutron noise appear both in the fast and the thermal group, the transfer function is actually a 2×2 matrix. Although the noise source appears in both groups, in traditional systems one only measures the thermal noise, and hence the calculations were also aimed at only this quantity. In that case, the adjoint approach has the advantage over the direct Green's function that it is sufficient to use the second column of the adjoint matrix, which can be determined from a vector equation. This two-component quantity was called the adjoint function, with a fast and a thermal component, similarly to the flux. Using the direct Green's matrix, to calculate the thermal noise induced by perturbations in both the fast and the thermal group, one would need the second row of the Green's matrix, which cannot be determined from one single vector equation, rather the whole Green's matrix needs to be calculated.

In the present study, given the fact that fast systems will also be investigated, it will be interesting to calculate not only the thermal noise, but also the fast noise. Indeed, in Gen-IV systems with a fast spectrum, it may be either advantageous, or simply necessary, to use the fast noise, or both the fast and the thermal noise, for maximum performance. In that case the advantage of the dynamic adjoint disappears. Hence in the present work both the adjoint function (adjoint matrix) and the Green's matrix will be used, and in all cases both the fast and the thermal neutron noise will be calculated and compared.

The formulae used are as follows. The static equations for the direct flux read as

$$\begin{pmatrix} D_1\nabla^2-\Sigma_{a1}-\Sigma_R+\nu\Sigma_{f1} & \nu\Sigma_{f2} \\ \Sigma_R & D_2\nabla^2-\Sigma_{a2} \end{pmatrix}\begin{bmatrix}\phi_1(z)\\ \phi_2(z)\end{bmatrix}=0, \tag{24}$$

where all symbols have their usual meaning. The notation $\Sigma_1=\Sigma_{a1}+\Sigma_R-\nu\Sigma_{f1}$ will also be employed. Zero flux conditions will be used at the extrapolated boundaries, i.e. $\phi_i(0)=\phi_i(H)=0$ for a one-dimensional system lying between $z=0$ and $z=H$.

The static fluxes are given as

$$\phi_1(z)=\sin B_0 z \tag{25}$$

$$\phi_2(z) = \frac{\Sigma_R}{\Sigma_{a2} + D_2 B_0^2} \sin B_0 z \tag{26}$$

with $B_0 = \pi / H$. Here the normalisation was used that the maximum amplitude value of the fast flux is unity. As is known, the equations for the static adjoints $\phi^{\dagger}_{1,2}(z)$ are simply obtained by transposing the matrix on the l.h.s. of Eq. (24), and are not written out explicitly.

The equation for the direct Green's matrix is obtained by first turning to the noise equations with the usual procedure of linearisation and temporal Fourier transform.
The equation for the group noises reads as

$$\begin{pmatrix} D_1\nabla^2 - \Sigma_1(\omega) & \nu\Sigma_{f2}(\omega) \\ \Sigma_R & D_2\nabla^2 - \Sigma_2(\omega) \end{pmatrix} \begin{pmatrix} \delta\phi_1(z,\omega) \\ \delta\phi_2(z,\omega) \end{pmatrix} = \begin{pmatrix} S_1(z,\omega) \\ S_2(z,\omega) \end{pmatrix} \tag{27}$$

Here the noise sources S_1 and S_2 are defined in terms of the cross section fluctuations and the static flux in the form

$$S_1(z,\omega) = \left(\delta\Sigma_R(z,\omega) + \delta\Sigma_{a_1}(z,\omega) - \delta\nu\Sigma_{f_1}(z,\omega)\left(1 - \frac{i\omega\beta}{i\omega + \lambda}\right)\right)\phi_1(z) -$$

$$\delta\nu\Sigma_{f_2}(z,\omega)\left(1 - \frac{i\omega\beta}{i\omega + \lambda}\right)\phi_2(z) \tag{28}$$

and

$$S_2(z,\omega) = -\delta\Sigma_R(z,\omega)\phi_1(z) + \delta\Sigma_{a_2}(z,\omega)\phi_2(z) \tag{29}$$

The Green's matrix that connects the noise in the fast and thermal group with the fast and thermal noise sources can then be written as

$$\begin{pmatrix} D_1\nabla^2 - \Sigma_1(\omega) & \nu\Sigma_{f2}(\omega) \\ \Sigma_R & D_2\nabla^2 - \Sigma_2(\omega) \end{pmatrix} \begin{pmatrix} G_{11}(z,z',\omega) & G_{12}(z,z',\omega) \\ G_{21}(z,z',\omega) & G_{22}(z,z',\omega) \end{pmatrix} =$$

$$\begin{pmatrix} \delta(z-z') & 0 \\ 0 & \delta(z-z') \end{pmatrix} \tag{30}$$

where the usual notations $\Sigma_1(\omega) = \Sigma_{a1} + \Sigma_R + \frac{i\omega}{v_1} - \nu\Sigma_{f1}(\omega)$, $\Sigma_2(\omega) = \Sigma_{a2} + \frac{i\omega}{v_2}$ and $\nu\Sigma_{fi}(\omega) = \nu\Sigma_{fi}\left(1 - \beta\frac{i\omega}{\lambda + i\omega}\right)$ were introduced. Eq. (30) can be written in a symbolic notation as

$$\hat{\mathbf{L}}(z,\omega)\hat{\mathbf{G}}(z,z',\omega) = \hat{\mathbf{I}}\delta(z-z') \tag{31}$$

where $\hat{\mathbf{I}}$ is the 2×2 unit matrix.

From Eq. (31) the noise can be obtained as

$$\begin{pmatrix}\delta\phi_1(z,\omega)\\ \delta\phi_2(z,\omega)\end{pmatrix}=\int_0^H\begin{pmatrix}G_{11}(z,z',\omega) & G_{12}(z,z',\omega)\\ G_{21}(z,z',\omega) & G_{22}(z,z',\omega)\end{pmatrix}\begin{pmatrix}S_1(z',\omega)\\ S_2(z',\omega)\end{pmatrix}dz' \tag{32}$$

or, again in symbolic form, as

$$\delta\overline{\mathbf{\Phi}}(z,\omega)=\int\hat{\mathbf{G}}(z,z',\omega)\overline{\mathbf{S}}(z',\omega)dz' \tag{33}$$

The elements of the above Green's matrix express the transfer between the noise source and the induced noise in the various groups. Thus, G_{12} connects the effect of a noise source in the thermal group at space point z' to the noise induced at point z in the fast group. From here it is seen that for the determination of the thermal noise only, one needs the second row of the Green's matrix. However, this quantity alone cannot be determined from a simpler vector equation, having only two components, rather all four components of the Green's matrix need to be determined simultaneously. In our case, we will be interested in the noise in both the fast and the thermal group, hence we will need the full Green's matrix anyway.

Defining

$$G_i(z,z',\omega)=$$

$$=\frac{1}{D_1D_2(\nu^2+\mu^2)}\begin{cases}\dfrac{\sin\mu(H-z')\sin\mu z}{\mu\sin\mu H}-\dfrac{\sinh\nu(H-z')\sinh\nu z}{\nu\sinh\nu H} & z<z'\\ \dfrac{\sin\mu z'\sin\mu(H-z)}{\mu\sin\mu H}-\dfrac{\sinh\nu z'\sinh\nu(H-z)}{\nu\sinh\nu H} & z>z'\end{cases} \tag{34}$$

where

$$\mu^2=\mu^2(\omega)=-\frac{1}{2}\left(\frac{\Sigma_1(\omega)}{D_1}+\frac{\Sigma_2(\omega)}{D_2}\right)+$$

$$\frac{1}{2}\sqrt{\left(\frac{\Sigma_1(\omega)}{D_1}+\frac{\Sigma_2(\omega)}{D_2}\right)^2-\frac{4}{D_1D_2}\Big(\Sigma_1(\omega)\Sigma_2(\omega)-\Sigma_R\nu\Sigma_{f2}(\omega)\Big)} \tag{35}$$

and

$$\nu^2=\nu^2(\omega)=\frac{1}{2}\left(\frac{\Sigma_1(\omega)}{D_1}+\frac{\Sigma_2(\omega)}{D_2}\right)+$$

$$\frac{1}{2}\sqrt{\left(\frac{\Sigma_1(\omega)}{D_1}+\frac{\Sigma_2(\omega)}{D_2}\right)^2-\frac{4}{D_1D_2}\Big(\Sigma_1(\omega)\Sigma_2(\omega)-\Sigma_R\nu\Sigma_{f2}(\omega)\Big)}, \tag{36}$$

we have

$$G_{11}(z,z',\omega)=\Big(D_2\nabla^2-\Sigma_2(\omega)\Big)G_i(z,z',\omega) \tag{37}$$

$$G_{21}(z,z',\omega) = -\Sigma_R G_i(z,z',\omega) \tag{38}$$

$$G_{12}(z,z',\omega) = -\nu\Sigma_{f2}(\omega) G_i(z,z',\omega) \tag{39}$$

$$G_{22}(z,z',\omega) = \left(D_1\nabla^2 - \Sigma_1(\omega)\right) G_i(z,z',\omega). \tag{40}$$

The equations for the adjoint Green's function are given by the adjoint two-group frequency dependent diffusion operator. For the general case, the adjoint Green's function $\hat{\mathbf{G}}^{\dagger}(\overline{\mathbf{r}},\overline{\mathbf{r}}',\omega)$ is also a 2×2 matrix, whose elements are determined by the equation

$$\hat{\mathbf{L}}^{\dagger}(\overline{\mathbf{r}},\omega)\hat{\mathbf{G}}^{\dagger}(\overline{\mathbf{r}},\overline{\mathbf{r}}',\omega) = \hat{\mathbf{I}}\cdot\delta(\overline{\mathbf{r}}-\overline{\mathbf{r}}') \tag{41}$$

where $\hat{\mathbf{I}}$ is the 2×2 unit matrix and $\hat{\mathbf{G}}^{\dagger}(\overline{\mathbf{r}},\overline{\mathbf{r}}',\omega)$ is given as:

$$\hat{\mathbf{G}}^{\dagger}(\overline{\mathbf{r}},\overline{\mathbf{r}}',\omega) = \begin{pmatrix} \mathbf{G}_{11}^{\dagger} & \mathbf{G}_{12}^{\dagger} \\ \mathbf{G}_{21}^{\dagger} & \mathbf{G}_{22}^{\dagger} \end{pmatrix} \tag{42}$$

and

$$\hat{\mathbf{L}}^{\dagger} = \hat{\mathbf{L}}^{\mathbf{T}} \tag{43}$$

It can be shown that with the help of the adjoint Green's matrix, the noise can be expressed as

$$\delta\overline{\mathbf{\Phi}}^{\mathbf{T}}(\overline{\mathbf{r}},\omega) = \int_{\mathbf{V_R}} \overline{\mathbf{S}}^{\mathbf{T}}(\overline{\mathbf{r}}',\omega)\hat{\mathbf{G}}^{\dagger}(\overline{\mathbf{r}}',\overline{\mathbf{r}},\omega)\mathbf{d}\overline{\mathbf{r}}' \tag{44}$$

where $\delta\overline{\mathbf{\Phi}}^{\mathbf{T}}(\overline{\mathbf{r}},\omega)$ and $\overline{\mathbf{S}}^{\mathbf{T}}(\overline{\mathbf{r}}',\omega)$ denote row vectors.

Eq. (44) shows that in order to determine the fast and the thermal noise, one needs to know the first and the second column of the adjoint Green's matrix, respectively. These can be calculated from a single vector equation each, and this constitutes a certain advantage when only one of two group noises is to be determined. So far only the thermal noise was of interest, which can be calculated by the second column of the adjoint Green's matrix (Pázsit and Demazière (2011)). This vector is called, somewhat misleadingly, the "adjoint function" in the literature, with its two components being called the "fast adjoint" and the "thermal adjoint". In this terminology the fast adjoint means the transfer between the *noise source in the fast group* and the thermal noise, and the thermal adjoint the transfer between the *thermal noise source* and the thermal noise. In our general notations here, $G_{ij}^{\dagger}$ stands for the transfer from the noise source in group i to the neutron noise in group j.

Since we will calculate both the fast and the thermal noise, neither the direct nor the adjoint Green's function technique will have any advantage over the other. Actually, as it is also easy to show, the direct and adjoint Green's functions obey the relationship

$$G_{ij}^{\dagger}(z,z',\omega) = G_{ji}(z',z,\omega) \tag{45}$$

Table 9 Steady-state parameters for each reactor type

Parameter	MOX	PWR	BWR	CANDU
H [cm]	367.0	365.8	368.0	594.0
D_1 [cm]	1.4719	1.4375	1.7986	1.4068
D_2 [cm]	0.5364	0.3723	0.4342	0.8696
$\nu\Sigma_{f1}$ [cm^{-1}]	0.0189	0.0056	0.0039	0.0007
$\nu\Sigma_{f2}$ [cm^{-1}]	0.2839	0.1405	0.0740	0.0084
Σ_{a1} [cm^{-1}]	0.0168	0.0112	0.0074	0.0011
Σ_{a2} [cm^{-1}]	0.2818	0.1022	0.0581	0.0057
Σ_R [cm^{-1}]	0.0083	0.0151	0.0131	0.0100
λ [s^{-1}]	0.0860	0.0881	0.0848	0.0848
β	0.0040	0.0054	0.0058	0.0058
v_1 [cm/s]	5.0806×10^{7}	1.8222×10^{7}	1.7549×10^{7}	4.3740×10^{9}
v_2 [cm/s]	2.8216×10^{5}	4.1388×10^{5}	3.9040×10^{5}	2.4190×10^{6}

Since in the simple model considered here (a homogeneous bare core), a solution can be obtained which is analytical in both arguments z and z', the two functions are equivalent in all respect. In the illustrations which follow both will be used, the selection simply depending on which one brings out the phenomenon to be shown in a more effective way.

2.3 Description of the systems used in the study

As mentioned in the introduction, we will investigate the dynamic response of four different cores to various perturbations. These selected systems correspond to four different existing or planned reactor types, and they constitute a wide range of neutron spectra. Starting from the hardest spectrum to the softest, these systems are

- a MOX fuelled fast reactor
- a PWR
- a BWR
- a heavy water core (representing a CANDU).

The fact that the PWR has a harder spectrum than the BWR may appear somewhat surprising. The difference between these two cores is relatively small, and which of the two has harder or softer spectrum depends on the actual core loadings.

Material parameters, corresponding to these four different systems are given in Table 9. Here, the notation MOX stands for a fast system with MOX fuel, whose data were taken from (Yoshioka (1998)); the PWR and BWR data are generic data corresponding to Swedish LWRs; finally CANDU stands for a thorium+plutonium loaded heavy water reactor.

The modelling of the perturbation, as seen in Eqs. (28) and (29), requires the knowledge of fluctuations of the various macroscopic two-group cross sections. We assume that the

Table 10 Cross section perturbations induced by a small (1oC) perturbation in the coolant inlet temperature for the four different reactor types.

Parameter	MOX	PWR	BWR	CANDU
$\delta\nu\Sigma_{f1}$ [cm^{-1}]	-2.8×10^{-6}	-2.8×10^{-6}	-5.0×10^{-6}	-2.8×10^{-6}
$\delta\nu\Sigma_{f2}$ [cm^{-1}]	-5.0×10^{-5}	-5.0×10^{-5}	-2.8×10^{-5}	-5.0×10^{-5}
$\delta\Sigma_{R}$ [cm^{-1}]	-5.2×10^{-5}	-5.2×10^{-5}	-1.2×10^{-4}	-5.2×10^{-5}
$\delta\Sigma_{a1}$ [cm^{-1}]	-5.0×10^{-6}	-5.0×10^{-6}	-1.5×10^{-5}	-5.0×10^{-6}
$\delta\Sigma_{a2}$ [cm^{-1}]	-6.0×10^{-5}	-6.0×10^{-5}	-5.8×10^{-5}	-6.0×10^{-5}

propagating perturbation in all four reactors, including the BWR, consists of the inlet temperature fluctuations of the coolant, and the corresponding variations of all the cross sections were calculated by using system codes. This constitutes a novelty as compared to most of the previous work in the field. In a one-group approach, in most works, it was assumed that a particular perturbation manifests itself in the change of one single cross section. The two most important applications have been the vibration of control rods and the effect of inlet temperature fluctuations of the coolant, both referring to PWRs. In both cases it was assumed that only the absorption cross section is perturbed, and immediate assumptions could be made on the analytical form of the space and frequency dependence of $\delta\Sigma_a(z,\omega)$. Only the functional form of the expression, but not its magnitude was of interest, in order to extract the necessary information (such as to locate the position of a vibrating absorber). In the case of boiling water reactors, only the perturbation of the removal cross section was considered, hence again it was sufficient to define $\delta\Sigma_R(z,\omega)$ as a propagating perturbation, again without any need of specifying its magnitude.

In the present case, the change in all cross sections was calculated for a change of 1^{o}C. The choice of this temperature change is of course arbitrary, hence the overall magnitude of the cross section fluctuations still can be left arbitrary. However, the relative amplitudes of the various cross section fluctuations in relation to each other are correctly determined, which hence provides a realistic modelling of such a perturbation. As it will be seen, the internal relationships of the various cross section perturbations have an influence on the induced noise. These internal relationships were determined by using the in-core fuel management neutronic system code SIMULATE-3 (Studsvik Scandpower (2001)) to determine the change of the various two-group cross sections to a unit change in the coolant temperature. This is given in Table 10.

2.4 Static fluxes

The static fast and thermal fluxes, with the maximum of the fast flux normalised to unity, are shown in Fig. 16 for all four systems. The static adjoints, with a similar normalisation, are shown in Fig. 17. The static fluxes show clear spectral differences, and they demonstrate that the sequence of fast to thermal systems is as described in the previous section, with the MOX loaded fast system having the hardest and the heavy water moderated CANDU reactor the softest. As expected, the static adjoints, showing the importance of the fast and thermal source neutrons, show a reversed sequence of the spectral characteristics.

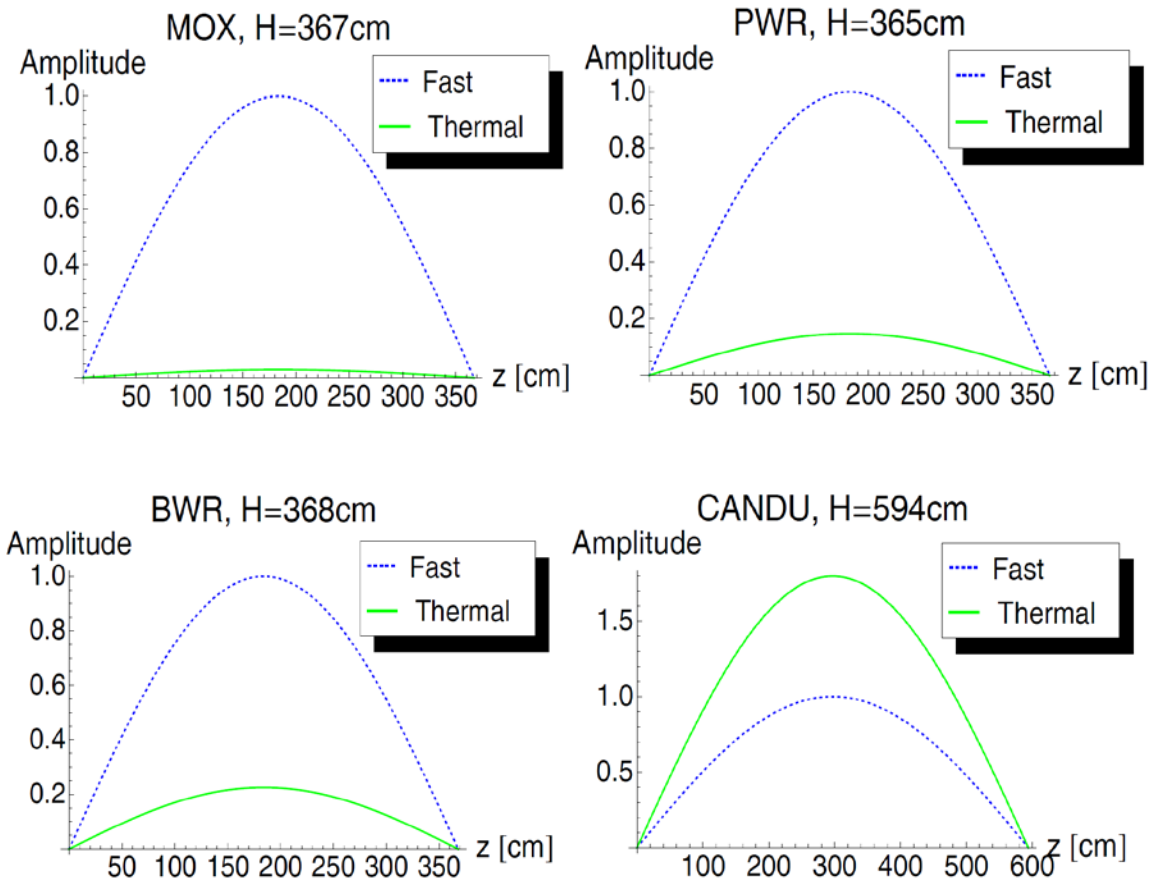

Fig. 16 Normalised static fluxes for: a fast reactor with MOX fuel (upper left figure); PWR (upper right figure); BWR (lower left figure); and CANDU reactor (lower right figure)

2.5 Frequency dependence of the adjoint Greens fluxes

The frequency dependence of the four components of the Green's matrix is shown in Fig. 18 for $z = z' = H / 2$, i.e. a central perturbation and central detector. These plots show a close resemblance to those in (Jonsson and Pázsit, 2011) which referred to MSR cores with similar spectral properties. The frequency dependence of the Green's functions follows that of the zero power reactor transfer function. As expected, the upper break frequency is lower for the heavy water moderated CANDU reactor than for the other cores. It is also seen that the four components are separated into two groups. The components G_{11} and G_{12}, which represent the noise in the fast group induced by fast and thermal noise sources, respectively, have a similar amplitude, and they are separated from the components G_{21} and G_{22}, which represent the thermal noise, and which also have similar amplitudes. The relationship between the amplitudes of these two groups follows that of the spectral ratio between the static fluxes. The separation between the two fast noise components and the two thermal noise components is largest for the MOX core, then it gradually decreases for the PWR and the BWR cores. For the CANDU core, the thermal noise is larger than the fast noise.

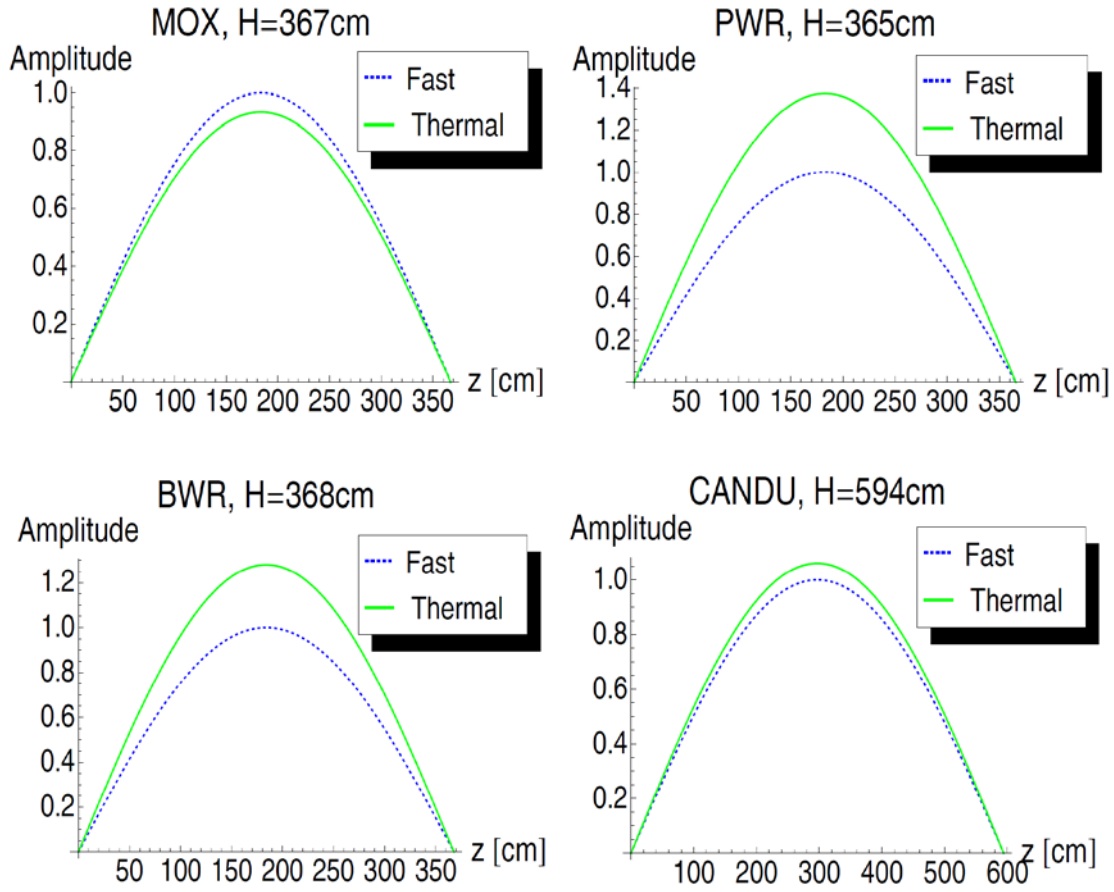

Fig. 17 Normalised static adjoints for: a fast reactor with MOX fuel (upper left); PWR (upper right); BWR (lower left); and CANDU reactor (lower right)

These results show that even for the light water cores, but in particular for the fast spectrum core, the neutron noise induced by a unit strength perturbation (either in the fast or in the thermal group) is significantly larger in the fast group than in the thermal group. For the MOX core the fast noise is more than an order of magnitude larger than in the thermal group. This indicates that even if detection of the fast neutrons is far less effective than that of the thermal neutrons, in fast reactors the use of the fast neutron noise could be a very useful complement to that of the traditional thermal neutron noise.

It is also interesting to note that in the fast and light water reactors, the frequency dependence of the component G_{22} deviates from that of the other three components at high frequencies (above the upper break frequency). It does not decrease as $1/\omega$ as the other three components do, its decay is much slower. The reason for this is the presence of the local component. Since the plots in Fig. 18 show the Green's functions components at $z = z'$, the detection point is at the maximum of the local component (cf. Fig. 20 in the next Subsection). As it is known from the literature, and which is also easy to see from Eqs. (35) and (36), the break frequency of the local root $\nu^2(\omega)$ is very much higher than that of the global root $\mu^2(\omega)$, and is practically constant at the global break frequency β / Λ. Hence, when the amplitude of the global component decreases below the local component, this latter will determine the amplitude which remains nearly constant. This is the same phenomenon as the behaviour of the phase of the

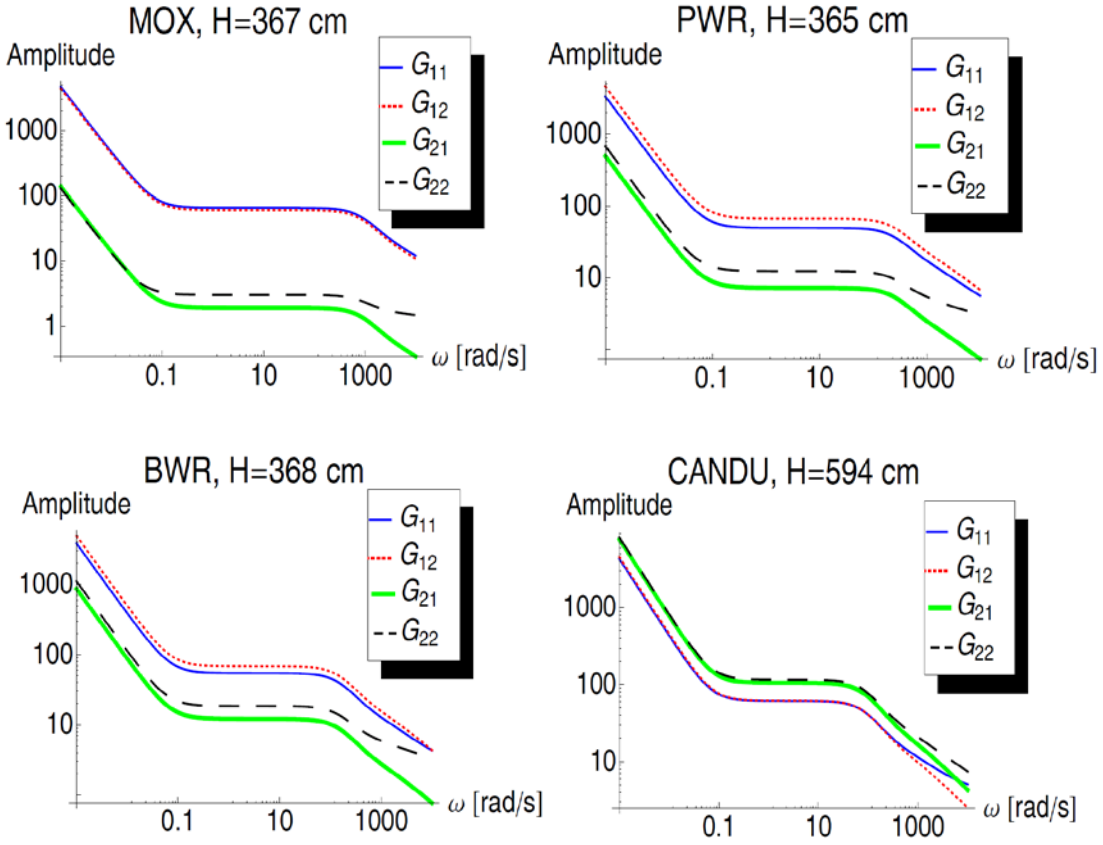

Fig. 18 Frequency dependence of the amplitude of the direct Green's function components: MOX (upper left figure), PWR (upper right figure), BWR (lower left figure) and CANDU reactor (lower right figure)($z = z' = H / 2$).

neutronic response in a reactor oscillator experiment in the Norwegian heavy water reactor NORA, as described in Bell and Glasstone (1970).

Curiously, for the case of the CANDU core, in addition to the component G_{22} whose high frequency behaviour deviates from the others, even that of the component G_{11} deviates to the same direction, even more visibly than G_{22}. This is in correspondence with the fact that for the CANDU case, there appears to be a small local component both in G_{11} and G_{22}. This is seen in Figs. 19 and 20. These show the adjoint Green's functions, but as was mentioned the diagonal components are equivalent with the direct Green's functions.

2.6 Space dependence of the adjoint Green's functions

Since in most work in the past the nature of the local component, and hence the space dependence of the transfer functions was performed by using the dynamic adjoint, in this subsection we will also use the components of the adjoint matrix. As mentioned earlier, in the past only the thermal neutron noise was of interest, for whose calculation it was sufficient to use the second column of the adjoint matrix. Here we will display the first and the second column of the adjoint matrix separately. The two components of

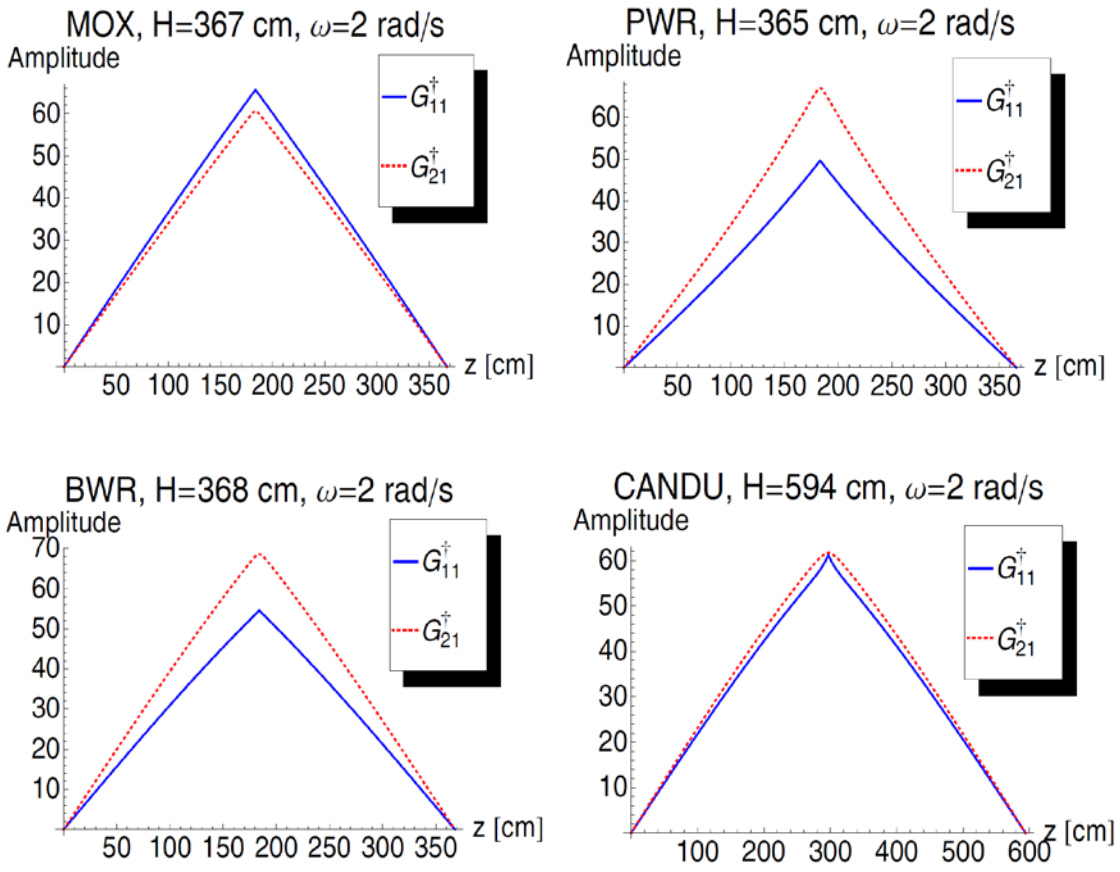

Fig. 19 Space dependence of the amplitude of the components of the fast adjoint: MOX (upper left figure) , PWR (upper right figure), BWR (lower left figure) and CANDU reactor (lower right figure) for $\omega = 2$ *rad/s and* $z' = H / 2$.

the first column, $G_{11}^{\dagger}$ and $G_{21}^{\dagger}$ give the fast neutron noise induced by a localised perturbation in the fast and the thermal group, respectively, whereas the two components of the second column, $G_{12}^{\dagger}$ and $G_{22}^{\dagger}$ give the same for the thermal noise. It is these two components which correspond to the components $\Psi_1^{\dagger}$ and $\Psi_2^{\dagger}$ of the so-called thermal adjoint. Again, in correspondence with the literature, the quantitative work will be restricted to the plateau frequency region $\lambda < \omega < \beta / \Lambda$. The frequency value $\omega = 2$ rad/sec will be used throughout.

The space dependence of the amplitude of the components of the fast adjoint function is shown in Fig. 19. Since the figure shows the case of power reactors at the plateau region, there is a seeming deviation from the point kinetic behaviour. In these Green's function components there is no visible occurrence of the local component, except, as was mentioned, in $G_{11}^{\dagger}$ of the CANDU core. It has to be added that the range of the local component (equal to the thermal diffusion length) is much larger in a heavy water system than in a light water reactor. Hence the local component is much less “local” in a CANDU reactor than in an LWR, which also makes it more difficult to discern it from the plot of the adjoint Green's function.

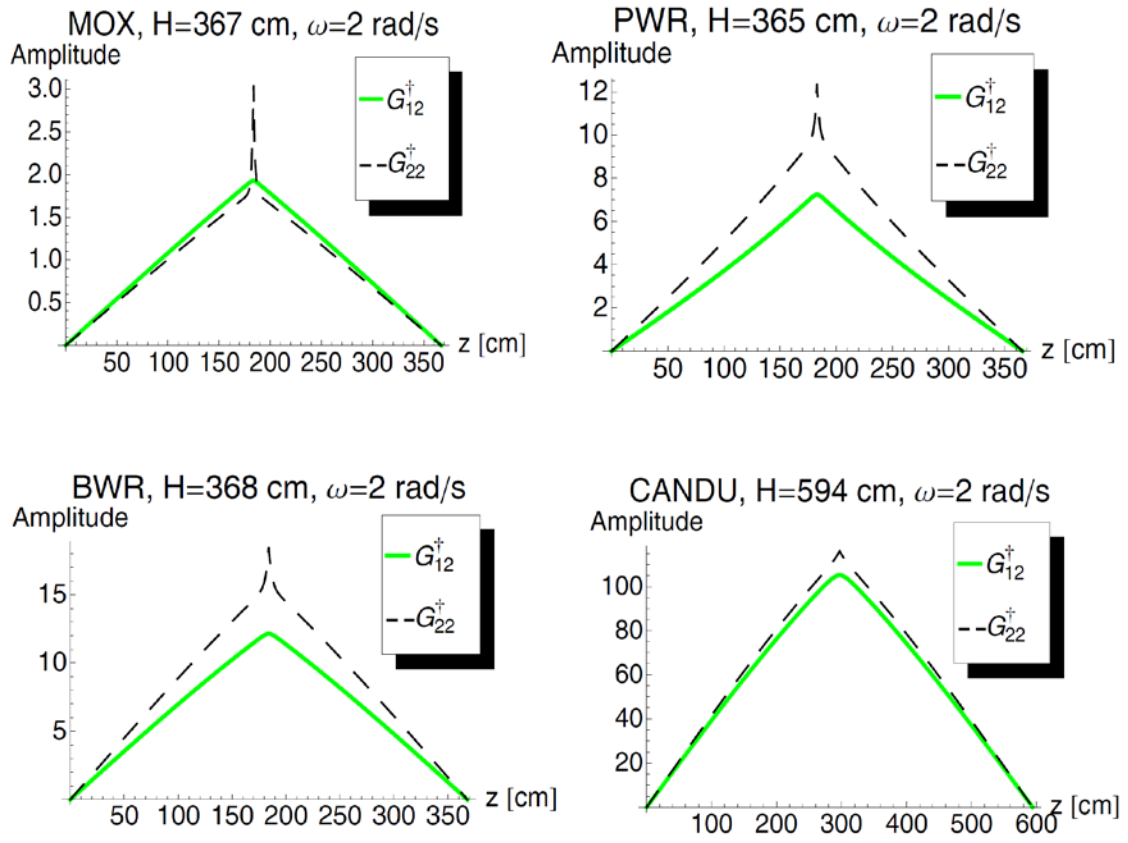

Fig. 20 Space dependence of the amplitude of the components of the thermal adjoint: MOX (upper left figure), PWR (upper right figure), BWR (lower left figure) and CANDU reactor (lower right figure) for $\omega = 2$ *rad/s and* $z' = H / 2$.

The space dependence of the amplitude of the thermal adjoints for the four cores is shown in Fig. 20. These show a resemblance to earlier calculations in the literature and for the fast and the light water cores clearly display a strong local component. The local component is the largest for the fast spectrum core. Somewhat surprisingly it is hardly visible for the CANDU core. One reason could be the earlier mentioned large range of the local component in heavy water systems, which makes the presence of the local component more difficult to see on the plot; but even so, the local component appears to have a smaller weight in HWRs than in LWRs. There appear to be no reported calculations in the literature of the transfer or adjoint function of CANDU cores, hence it is not possible to say whether this observation agrees or disagrees with other work in the field.

2.7 Investigation of the propagation noise

The main motivation for the present study was to investigate the space and frequency dependence of the propagation noise, i.e. the neutron noise induced by a propagating perturbation, in systems of various spectral properties, and whenever feasible, compare it with the result of similar calculations performed recently by Jonsson and Pázsit (2011). The origin of the interest in propagation noise lies in the characteristics of the neutron noise induced by inlet temperature fluctuations propagating with the coolant of a PWR, and the noise induced by the two-phase flow, propagating with the coolant of a BWR.

The recent interest arose in connection with molten salt reactors where density and material inhomogeneities may propagate with the molten salt and hence can give rise to neutron noise.

As usual, the temperature, void etc. perturbations are represented by the fluctuations of some group constants. The propagating property is expressed as

$$\delta\Sigma(z,t) = \delta\Sigma(z=0, t - z\,/\,v) \tag{46}$$

where v is the velocity of the propagation. In the frequency domain, (46) will read as

$$\delta\Sigma(z,\omega) = \delta\Sigma(z=0,\omega)e^{-i\omega\frac{z}{v}} \tag{47}$$

This form is then substituted into the expressions for the noise source, Eqs. (28) and (29), which then in turn can be integrated either with the direct Green's function as in (33) or with the adjoint Green's function, Eq. (44), to obtain the group noises. These two methods are completely equivalent and require identical effort. In this work the adjoint function was used to calculate the noise, without any specific reason.

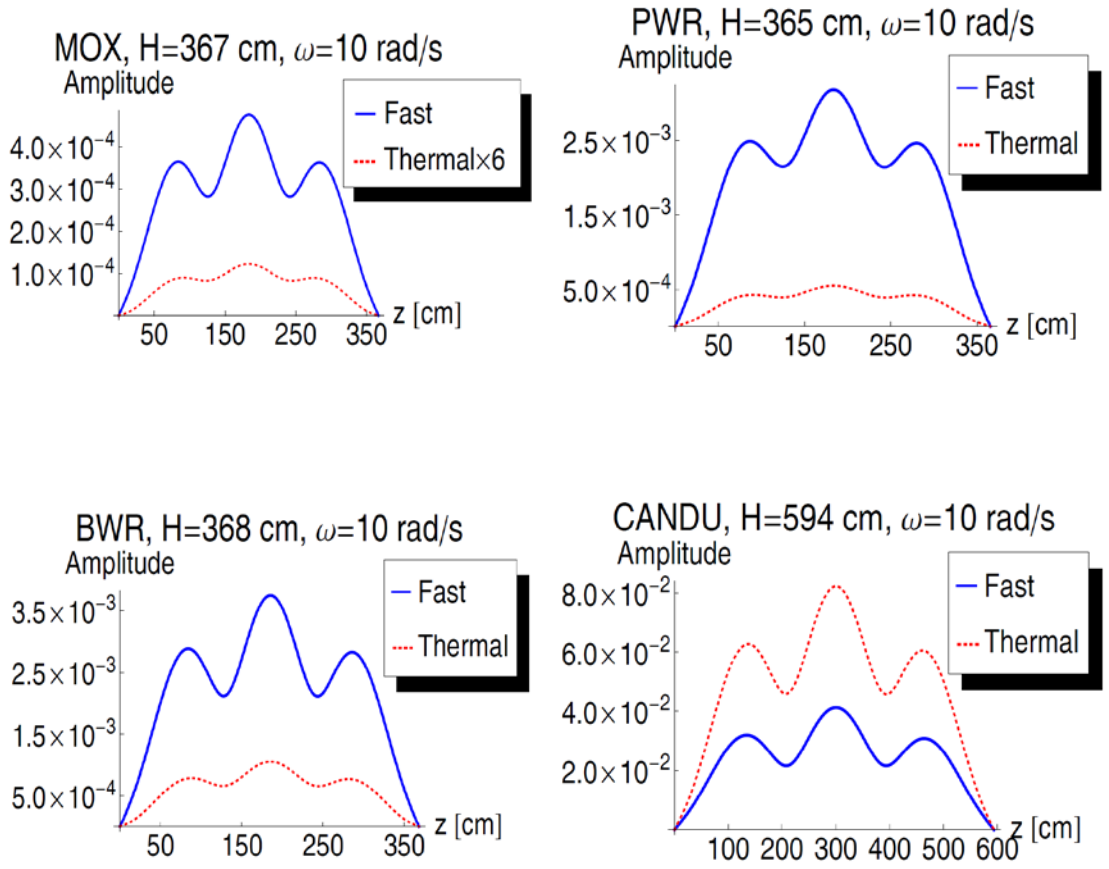

Fig. 21 Space dependence of the neutron noise induced by propagating perturbation of the thermal absorption cross-section only: in a MOX (upper left figure), in a PWR (upper right figure), in a BWR (lower left figure) and in a CANDU reactor (lower right right figure) for rad/s and cm/s. For the MOX core, the thermal noise was multiplied by a factor 6 for better visibility.

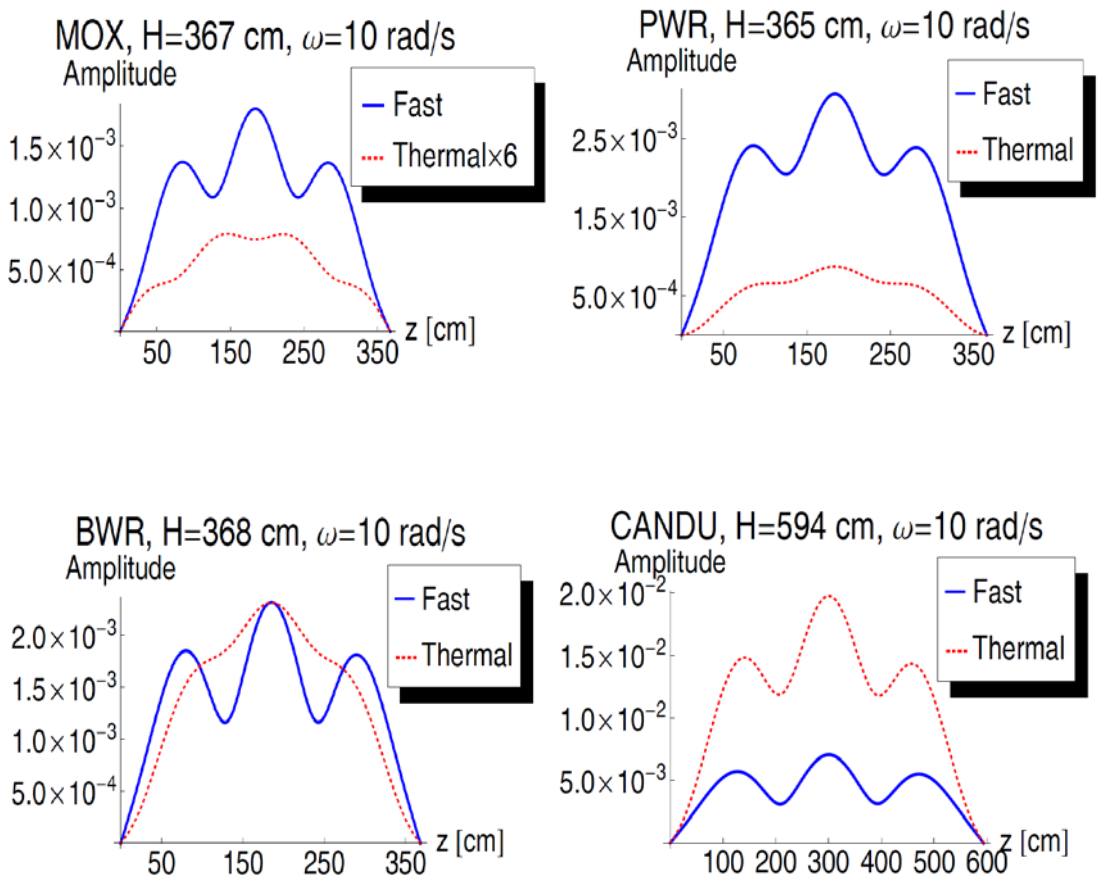

Fig. 22 Space dependence of the propagation noise induced by the fluctuations of all cross-sections in the four cores considered, for $\omega = 10$ rad/s and $v = H / 2$ cm/s. For the MOX core, the thermal noise was multiplied by a factor 6 for better visibility.

2.7.1 Space dependence of the propagation noise

The noise calculations will be performed and discussed in two steps. First, it will be assumed that only the thermal absorption cross section is perturbed. This is because we want to relate the results to earlier ones in the literature, and these were so far always calculated by considering the perturbation of only one cross section, either that of the thermal absorption cross section or the removal cross section. This is necessary for such a comparison since, as it will be seen shortly, when taking into account the case of several cross sections being perturbed, the structure of the propagation noise is significantly changed.

The space dependence of the fast and thermal propagation noise induced by fluctuations of the thermal absorbing cross section is shown in Fig. 21 for the four core types investigated. These plots have a form similar to those of the one-group calculations of Pázsit and Dykin (2010) in a PWR and the two-group calculations of Pázsit and Jonsson (2010) in molten salt systems. The reason for the spatial oscillations of the noise is the same as described in the previous publications, i.e. an interference phenomenon between the point kinetic and space dependent components. The spatial structure of the fast and the thermal noise is the same, which is also in accordance with the previous

results. It is seen that the spectral ratio of the noise is similar to that of the static fluxes and can be also directly related to the spectral ratio of the corresponding elements of the direct Green's function (Fig. 18). For the MOX core the thermal noise is vanishingly small as compared to the fast noise, and the thermal noise was multiplied in the figure with a factor 6 for better visibility.

The strong spatial tilt of the space dependence of the noise, observed in several cases of MSR calculations, published in (Pázsit and Jonsson (2010)) cannot be seen here. This effect seems therefore to be related to the propagating fuel, or the material properties of other cores such as thorium loaded ones.

The space dependence of the propagation noise as induced by perturbations of *all* cross sections is shown in Fig. 22. The fluctuations of the individual cross sections were calculated by the ICFM system code SIMULATE-3 by considering the perturbation of the inlet coolant temperature in both the PWR and the BWR core. Since, unlike for the PWR and BWR case, we have access neither to system codes nor to input decks, no similar calculations were performed for the fast MOX system and the thermal CANDU core. Instead, the same internal ratio of the various cross section perturbations was used as for the PWR. In view of the fact that a significant difference was found between the cases when the fluctuation of only one cross section generates the neutron noise and when the fluctuation of several cross section is taken into account, and in view of the fact that the latter corresponds to the real case much better, it would be advisable to perform similar calculations for fast and heavy water systems as well. Fast systems can be treated by the system code ERANOS, whose application to this problem is planned in later work.

The characteristics of the propagation noise show a number of interesting features. The fast noise looks similar to that of the previous case, but the thermal noise displays several differences. One of these is the case of the MOX core, where the oscillating structure of the thermal noise is changed and is not the same any longer as that of the fast noise. The maxima and the minima changed place, and the spatial oscillations of the fast and the thermal noise are out of phase.

The explanation is that when fluctuations of several cross sections take place simultaneously, their effect adds up with different signs and different weights in the resulting noise. The sign differences can be seen in Eqs. (28) and (29). These are simply due to the fact that different processes contribute differently to the neutron balance, through representing generation or destruction of the neutrons in the corresponding groups. The different weighting is related to the fact that the fast and thermal noise sources are contributing to the propagation noise through a weighting by the different components of the Green's function (Eq. (33)) (or, equivalently, by the components of the adjoint Green's function). As was seen earlier, the amplitude of different components shows also a significant variation. Moreover, the phase of the different Green's function components is also different. All these factors contribute to the fact that the structure of the propagation noise (and also that of the neutron noise induced by other perturbations) is more complicated for the case when the fluctuation of all cross sections is taken into account. This will be more visible and discussed further in the next subsection.

Another difference between Fig. 21 and Fig. 22 is that in the latter, the thermal noise is much larger in the BWR than in the case of pure thermal absorption cross section

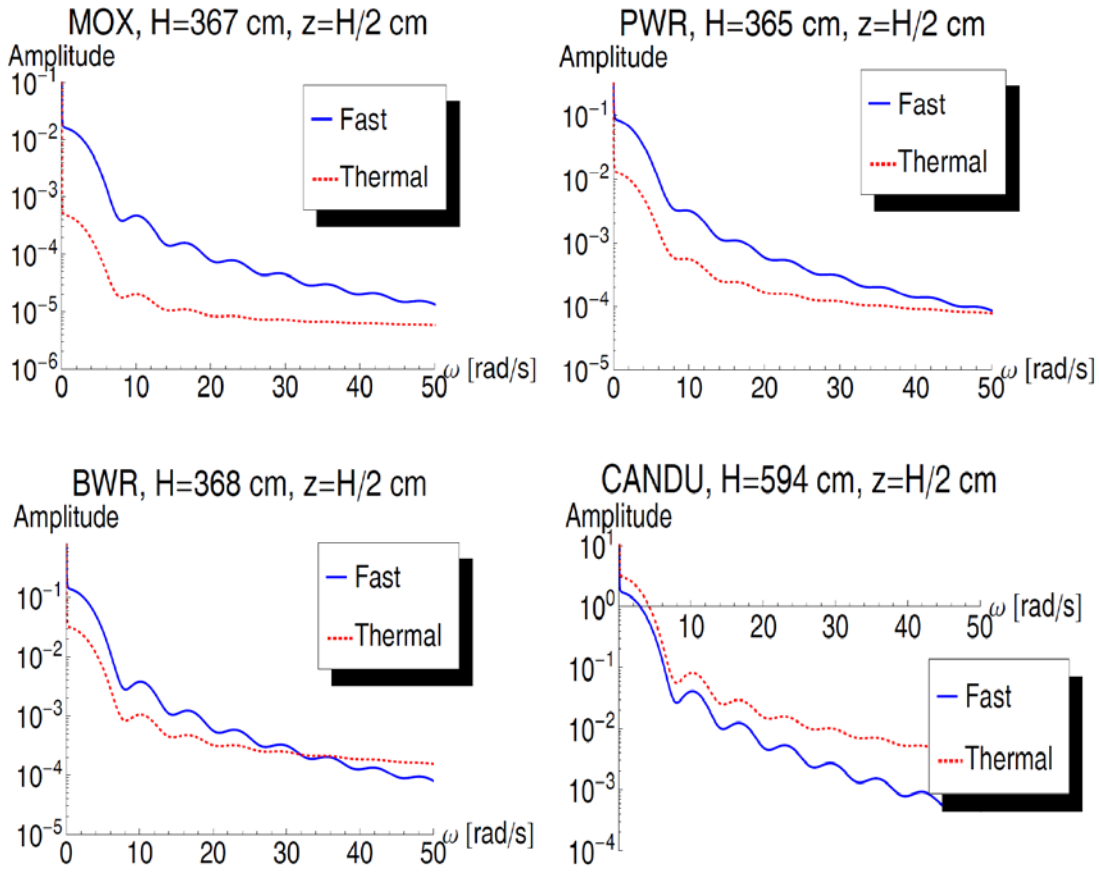

Fig. 23 Frequency dependence of the neutron noise induced by propagating temperature perturbation in absorption cross-section only in MOX reactor (upper left figure), in PWR (upper right figure), in BWR (lower left figure) and in CANDU reactor (lower right figure) for $z = H/2$ *cm and* $v = H/2$ *cm/s.*

perturbations. The explanation is that unlike in the other cores, in the BWR, an increase of the coolant temperature leads to an increase of the void fraction, with the result that the change in the removal cross section becomes much larger than that of the thermal absorption cross section. On its turn, perturbation of the removal cross section affects the thermal noise much more than the fast noise, although the pure contribution from the removal cross section is comparable for the fast and the thermal noise. This is because in the thermal noise, the component due to the removal cross section dominates over the noise induced by the other cross section fluctuations. In the fast noise, the noise induced by the removal cross section and the noise by the other cross section fluctuations are of comparable magnitude but opposite phase, hence there is no increase of the noise by adding the fluctuations induced by the removal cross section.

2.7.2 Frequency dependence of the propagation noise

The same sequence will be followed here as for the space dependence. First the frequency dependence of the amplitude of the propagation noise, induced solely by the fluctuations of the thermal absorption cross section, will be calculated. The result is shown in Fig. 23 for the four cores.

Several features of these spectra show similarities with the corresponding MSR calculations by Jonsson and Pázsit (2011). One is the spectral ratio of the noise, which also follows from the results shown earlier in this paper for the Green's functions (Fig. 18) and the space dependence of the propagation noise (Fig. 21). Two further such features are the somewhat deeper sinks in the fast noise than in the thermal noise, and the slower decay of the spectra with increasing frequency in the thermal noise than in the fast noise.

Both of these latter features depend on the fact that the thermal noise is affected by the presence of the local component, whereas the weight of the local component is vanishingly small in the transfer function components which are used to calculate the fast noise. Regarding the depth of the sinks, the local component, similarly to the pure space dependent component, does not have a sink structure, hence its presence makes the sinks relatively shallower. Concerning the decay of the spectra with increasing frequency, the part of the noise which is due to the local component, will decay slower than the global component (consisting of the sum of the reactivity and the space dependent part), for two reasons. One of these relates to the frequency dependence of the amplitude of the corresponding component of the transfer function. The amplitude of the local component decays much slower in frequency than that of the global component. This is the same phenomenon as the one behind the high frequency tail of

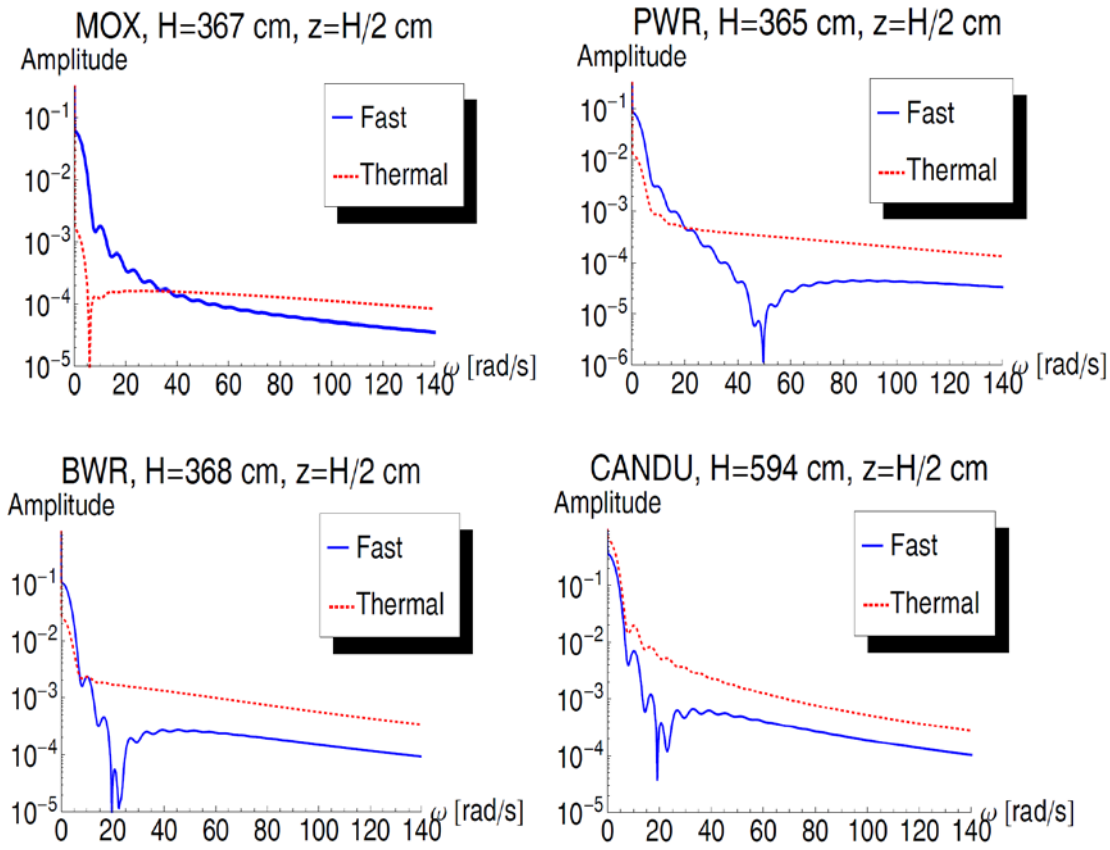

Fig. 24 Frequency dependence of the neutron noise induced by propagating temperature perturbation in MOX (upper left figure), in PWR (upper right figure), in BWR (lower left figure) and in CANDU reactor (lower right figure) for $z = H/2$ *cm and* $v = H/2$ *. cm/s.*

G_{22} described earlier. The other reason is related to the integral of the transfer functions with the noise source. As is seen from Eq. (47), the propagating perturbation represents a function which oscillates in space, and the oscillation frequency increases with increasing frequency. The integral of any smooth function with a more and more rapidly oscillating function decreases monotonically. This decrease is much faster for the global component, which varies smoothly in space with a relaxation length comparable with the core size, than for the local component, whose relaxation length is much shorter. These two effects together explain the slower decay of the thermal noise with increasing frequency as compared to the fast noise.

The next step is the calculation of the propagation noise, induced by the perturbation of the coolant temperature, affecting all cross sections, as described in the previous Subsection. The results are shown in Fig. 24.

The structure of these spectra is significantly more complicated and irregular than in the previous case when the noise was induced only by the fluctuations of the thermal absorption cross section. Some general properties are though preserved, although in a less clear form: the spectral ratio of the noise components, the less pronounced sink structure of the thermal noise, and its slower decay in frequency than that of the fast noise. These general features have the same reason as for the case of the noise generated only by one cross section fluctuations, shown in Fig. 23. However, the sink structure is much diminished and irregular even for the fast noise, and there are some peculiar deep dips in either the fast or the thermal noise at a given frequency in all systems. The frequency of this dip and its character is though different for the four different systems.

The seemingly irregular sink structure and the single deep sinks in the spectra can all be understood by considering the contributions of the various cross section fluctuations separately, and in some cases splitting the contribution further to components due to the local and the global components of the noise. Namely, the structure of the noise is the result of the interplay of these various components, and although each of them has

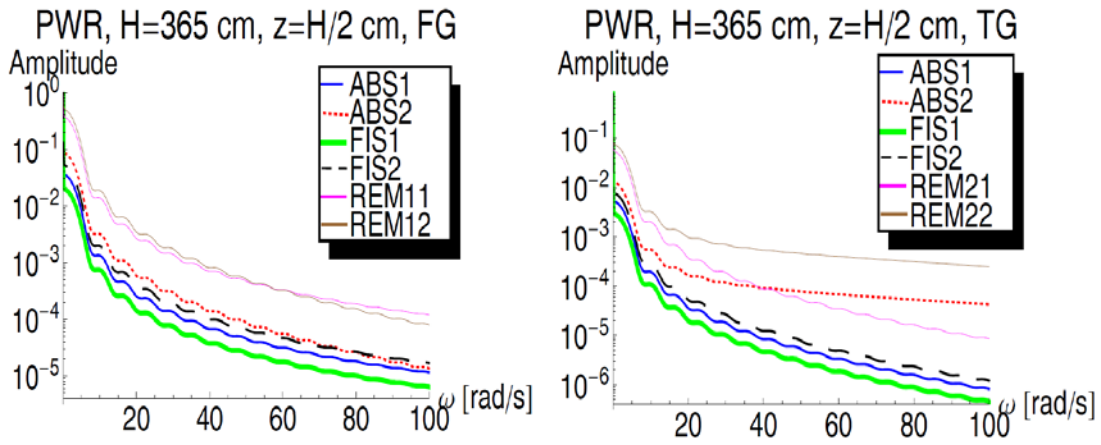

Fig. 25 Frequency dependence of the amplitude of the neutron noise induced by propagating temperature perturbation in ABS1, ABS2 FIS1, FIS2 and REM separately for a PWR in fast (left figure) and thermal (right figure) groups, respectively for $z = H / 2$ *cm.*

either a smooth or regular periodic structure, their interplay leads to the irregularly looking behaviour.

As an example, we shall take a closer look at the structure of the frequency dependence of the propagation noise for the case of a PWR shown in Fig. 24 (top right figure) where the amplitude of the fast noise has a deep sink around 50 rad/s. All cross sections are affected by the temperature fluctuations of the coolant: the absorption cross sections in the fast and thermal energy groups, the fission cross sections in the fast and thermal groups, and the removal cross section. We first split the total neutron noise into five components, each induced by the perturbation of one of the cross sections. The amplitude and the phase of the five components is shown in Figs. 26 and 25. For better visibility of the entire noise structure, the amplitudes are given separately in the left part of Fig. 26, whereas the right part of Fig. 26 represents only the most interesting parts of the curves.

The phase of the noise does not have much information except the phase relationship between the different components. Some components are in-phase, some out-of-phase.

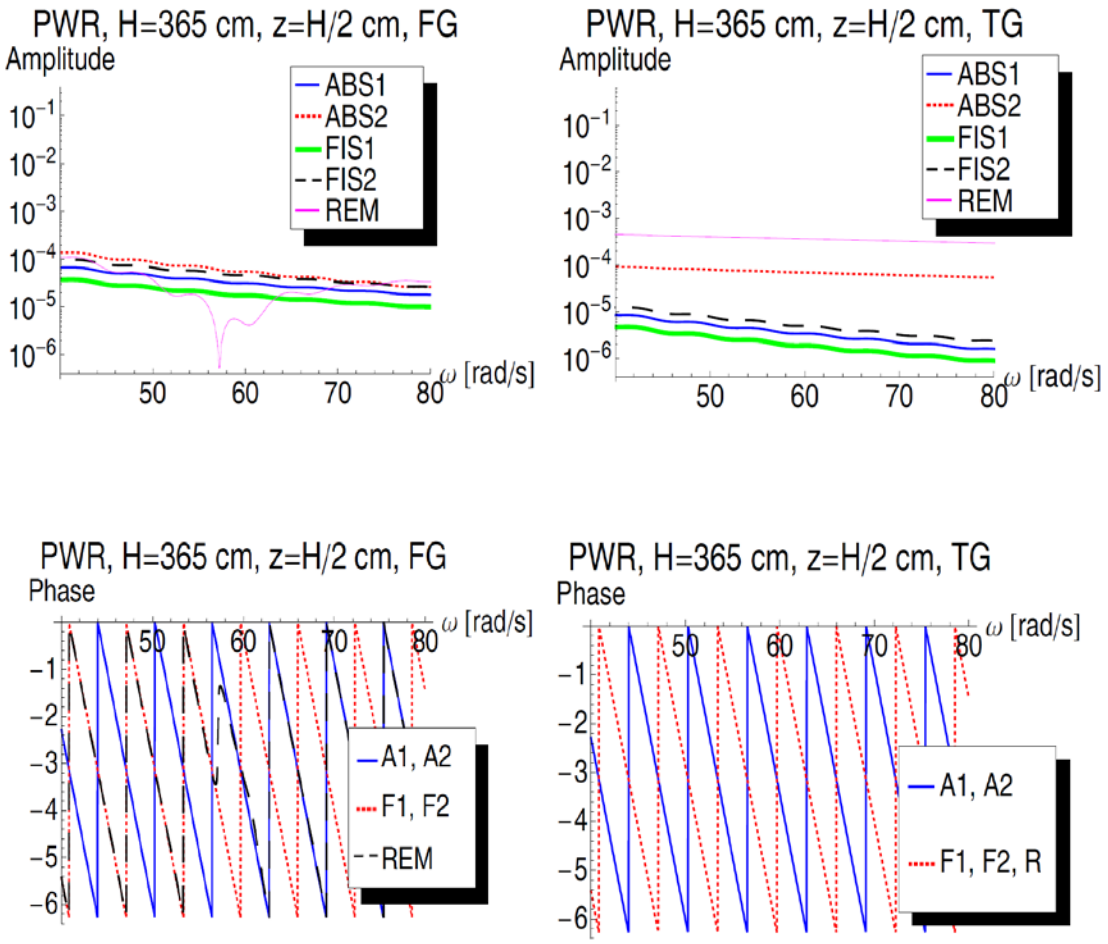

Fig. 26 Frequency dependence of the amplitude and phase of the neutron noise induced by propagating temperature perturbation in ABS1, ABS2 FIS1, FIS2 and REM separately for a PWR in fast (left figures) and thermal (right figures) groups, respectively for $z = H / 2$ *cm.*

The monotonically decreasing slope just follows that of the perturbation, as is discussed in (Pázsit and Dykin (2010)). The in- or out-of-phase property explains if there is a constructive or destructive interference between the different components of the noise.

There is more information in the amplitude of the noise components. As Fig. 26 (left figure) shows, each component, except the one induced by the removal cross section fluctuations, shows a regular sink structure, similar to that observed in earlier work. However, since some components are out-of-phase with each other, the sum of the components has a less pronounced sink structure. In addition, the position of the sink frequencies can also slightly vary for the different components, due to the different interplay of the reactivity and the space dependent components, which is due to differences in the corresponding Green's function components. It is also seen that, in particular in the thermal noise, some components decay slower than some others.

It is also seen that the similar deep sink, which is observed in the total fast noise in Fig. 24, is present in the noise component due to the removal cross section fluctuations. In order to understand the reason for this, we need to split even this component into further components. Since the fluctuations of the removal cross section appear in both the fast and the thermal noise source, two different components of the direct or adjoint Green's function are involved in the calculation of the neutron noise, taken with opposite sign. The large dip in the fast noise around 50 rad/s induced by the removal cross section is due to the interplay between these two Green's function components, but are even related to the local and the global components of the noise. This is illustrated first by splitting up the noise partly for the different Green's function components, i.e. G_{11} and G_{12}, and partly into local and global components. The splitting up of the noise for the two different Green's function components for the removal cross section is shown in Figs. 27 and 28. For the same reason as before, the amplitudes are given separately in Fig. 27 and 28.

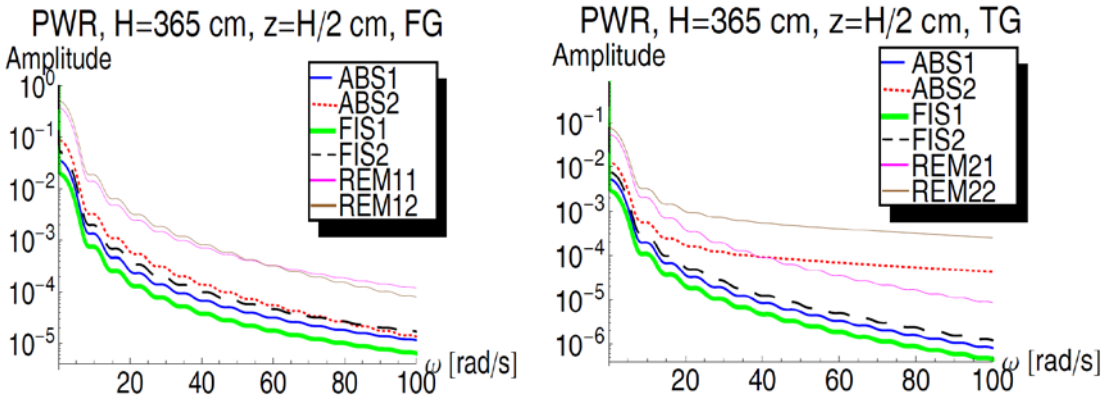

Fig. 27 Frequency dependence of the amplitude of the neutron noise induced by propagating temperature perturbation in ABS1, ABS2 FIS1, FIS2 and REM separately for a PWR in fast (left figure) and thermal (right figure) groups, respectively for $z = H/2$ cm (the component corresponding to the removal cross section is split into two components).

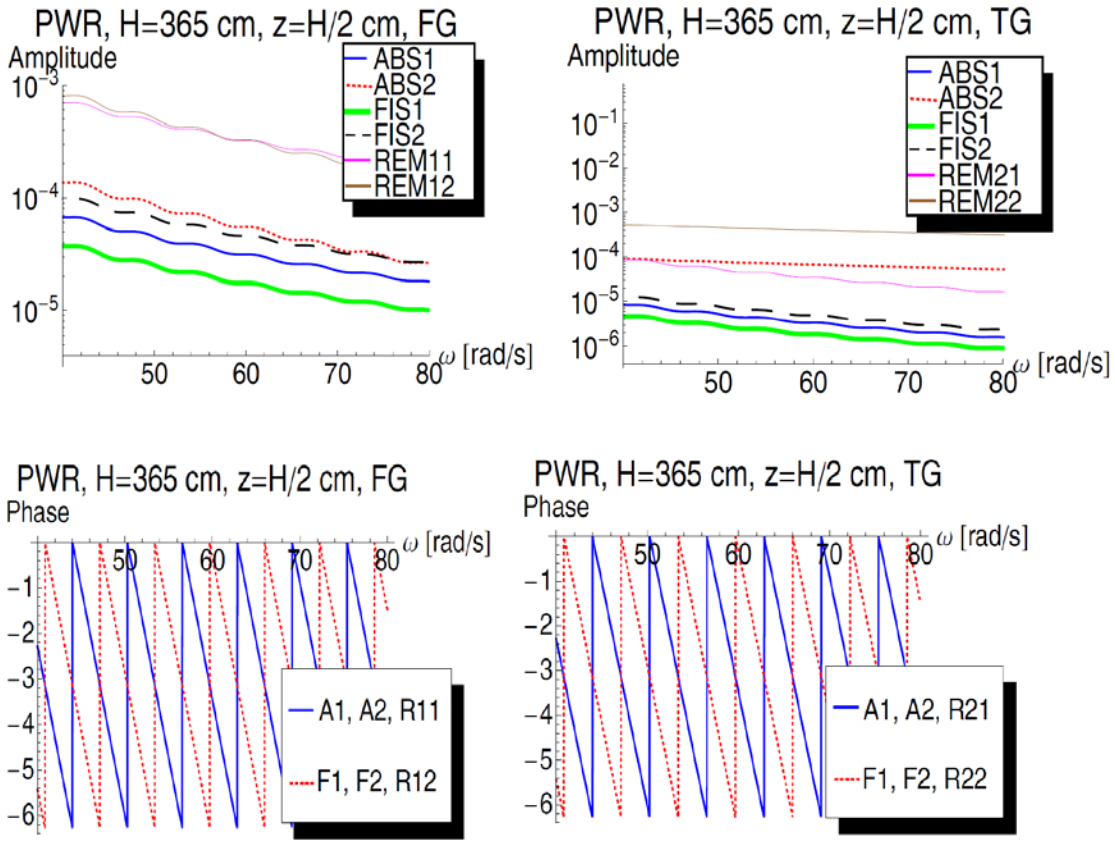

Fig. 28 Frequency dependence of the amplitude and phase of the neutron noise induced by propagating temperature perturbation in ABS1, ABS2 FIS1, FIS2 and REM separately for a PWR in fast (left figures) and thermal (right figures) groups, respectively for $z = H / 2$ cm (the component corresponding to the removal cross section is split into two components).

It is immediately seen that now all components are smooth periodic functions, even those belonging to the removal cross section. However, the two components, having approximately the same magnitude, are out of phase (this follows directly from the different sign of the removal component in the noise source, as seen from Eqs. (28) and (29), and moreover they decay slightly differently in frequency.

At the frequency where their amplitude becomes equal, a full destructive interference takes place. And since in the total noise the component belonging to the removal cross section is dominating, this leads to the deep sink seen in the total noise.

The different slope of the two components of the removal noise is, on the other hand related to the different weight of the local component in the two Green's functions. This is illustrated in Fig. 29 which shows the frequency dependence of the amplitude and the phase of the local and global components on the fast noise, contained in the Green's matrix elements G_{11} and G_{12}, respectively.

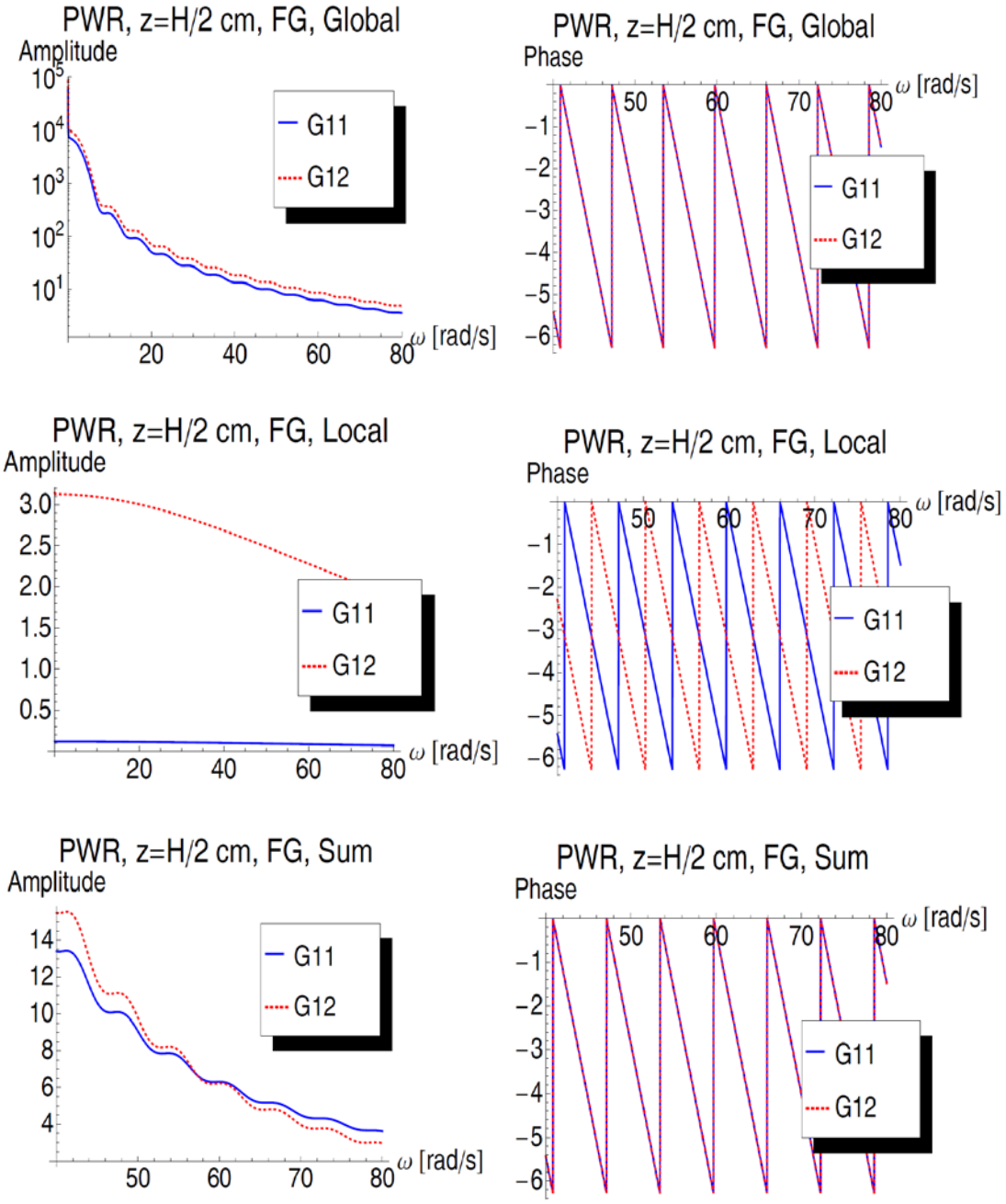

Fig. 29 Frequency dependence of the amplitude and the phase of the neutron noise induced by propagating temperature perturbation for a PWR for the global and local components and their sum in the fast group, respectively, for $z = H / 2$ *cm.*

It is seen that the global components of the neutron noise corresponding to the G_{11} and G_{12} components exhibit a similar structure and are almost equal in their amplitudes. At the same time, as already argued for it earlier, the frequency decay of the local component of the noise is very much slower that that of the global component, in addition of being also a smooth function in frequency. In addition, as the figure also shows, the local component of the noise is much larger in the term due to G_{12} than in

that due to G_{11}. Further, in the term due to G_{12}, the local component is out-of-phase with the global component. These facts together lead to the different slope of G_{11} and G_{12} such that at a certain frequency their magnitude becomes equal. Since the noise induced by the fluctuation of the removal cross section is due to $G_{11} - G_{12}$, this leads to the destructive interference, resulting in the dip in the fast noise around 50 rad/s.

With a similar analysis, it can be shown that there is no similar effect in the thermal propagation noise in the PWR. It is seen in the right part of Fig. 26 that there is no deep dip in any of the noise components, including the one corresponding to the removal cross section. The main reason is that in the noise due to the removal cross section and G_{22}, the local and the global components are in phase. Hence the slopes of the two components G_{21} and G_{22} are diverging, and do not become comparable at any frequency. With a similar analysis all features of the spectra in Fig. 24 can be explained, i.e. why the dip frequency is different for the different cores, and why the dip occurs in the thermal noise in the MOX system, whereas it appears in the fast noise in the other three systems.

The reason why the possibility of such a single deep sink was not observed for the case of power reactors, i.e. where the point kinetic behaviour does not dominate, depends mostly on the fact that it light water reactors it only occurs in the fast noise, which was not investigated so far. On the other hand it is seen from the study presented here that in cores with different parameters, such as the MOX core with a fast spectrum, the dip occurs in the thermal noise, and moreover at a relatively low frequency which is monitored by most core surveillance systems.

2.8 Conclusions, further work

The investigations presented here show that most of the properties of the fast and thermal propagation noise, found in recent work regarding molten salt reactors (Jonsson and Pázsit, 2011) is also present in traditional reactors, i.e. they are not a consequence of the propagating fuel and hence the propagating delayed neutron precursors and the accompanying difference in the dynamics of an MSR and a traditional core. These concern the spectral ratio of the neutron noise, the depth of the dips in the fast and thermal noise, and the decay of the amplitudes with increasing frequency. The spatially asymmetric characteristics of the noise could not be reproduced, which is a difference between the traditional systems investigated here and the MSR-type cores in the above publication.

One outcome of the quantitative work is that in particular in fast core systems, for a given propagating perturbation, the neutron noise is substantially larger in the fast group than in the thermal group. This observation might have a bearing on the use of noise diagnostic methods in fast systems such as an SFR. The results suggest that it is beneficial to include fast neutron detection methods in the noise diagnostic system in fast reactors.

The results presented in this paper also underline the fact that for describing perturbations which affect several cross sections simultaneously, it is essential that the

fluctuations in all cross sections are taken into account. This is the case at least when none of the cross section fluctuations dominates over the others. In BWRs, it was sufficient to consider only the fluctuations of the removal cross sections in order to have an in-depth understanding of the in-core noise. For the description of the noise related to temperature and density variations of one-phase low coolant, the present results suggest that it is necessary to model the noise source by accounting for its effect on all cross sections. This concern in particular molten salt reactors, in which propagating perturbations of various origin (temperature, density, fissile component etc.) are expected to occur. One can also add that the present findings add one more item to the list given in (Pázsit and Dykin, 2010) as to why the sink structure was never observed in the APSDs of in-core detectors in PWRs.

3 A consistent derivation of the point kinetic term of the noise in circulating fuel reactors and an analysis of the deviation from traditional systems

3.1 Introduction

In the theory of neutron noise in power reactors, the validity of the various kinetic approximations has a special significance regarding the possibilities for noise diagnostics. Whether a system behaves in a point kinetic or strongly space dependent manner, determines the possibilities of identifying and locating perturbations in the core, or to determine integral parameters from measurements in a single point.

However, derivation of the point kinetic equations for Molten Salt Reactors (MSR), is not as simple as for traditional reactors, due to the streaming term appearing in the precursor equations. Curiously, the solution for the full problem, i.e. the space- and frequency dependent neutron noise, can be given in a compact analytical form for the case of infinite fuel velocity. From the full solution, the point kinetic component can be calculated analytically by using simple orthogonality relations. This is performed in this work. It is shown that for an MSR the point kinetic component in the frequency domain cannot be factorized into the reactivity and a zero power transfer function; a slightly more complicated expression is obtained and discussed.

3.2 Basic considerations

The kinetic approximations are defined through the flux factorization in the form

$$\phi(x,t) = P(t)\psi(x,t) \tag{48}$$

with the usual normalization and boundary conditions. Splitting both the space-time dependent flux as well as the amplitude and shape function into static (expected) values and fluctuations, and using linear theory, in the frequency domain the neutron noise $\delta\phi(x,\omega)$ can be written as the sum of a point kinetic and a space dependent term as

$$\delta\phi(x,\omega) = \delta\phi(x,\omega)_{p.k.} + \delta\psi(x,\omega) = \delta P(\omega)\phi_0(x) + \delta\psi(x,\omega) \tag{49}$$

where $\delta P(\omega)$ can be further factorised as

$$\delta P(\omega) = G_0(\omega)\rho(\omega)\,. \tag{50}$$

Here $G_0(\omega)$ is the zero power reactor transfer function, and $\rho(\omega)$ the reactivity effect of the cross section fluctuations, defined by a first order formula. Under these assumptions the fluctuation $\delta\psi(x,\omega)$ of the shape function is orthogonal to the static flux. A detailed description of the assumptions and procedures can be found in (Pázsit and Demazière, 2011). The convergence to point kinetic behaviour, for perturbations with a non-zero reactivity effect, is the consequence of the fact that the transfer function $G_0(\omega)$ diverges in critical systems when the frequency tends to zero, whereas the space-dependent component $\delta\psi(x,\omega)$ remains finite.

Eq. (49) and (50) can be derived in a number of equivalent ways by using the flux factorization technique either in the original space-time dependent diffusion equations, or in the solutions in the frequency domain. However, in the case of an MSR, the noise factorization technique is not applicable in the standard form. It will be shown how the point kinetic component can be calculated and how the asymptotic convergence of the system to point kinetic behaviour arises at low frequencies.

3.3 General equations of an MSR

A one-dimensional reactor model will be considered along the x axis, which is also the direction for the flow of the liquid fuel, with boundaries at $x = \pm a$. The core size is $H = 2a$ with an external loop for the fuel recirculation of length L and with a total recirculation length $T = H + L$. The same fuel velocity u is assumed both within and outside the core.

The space-time dependent diffusion equations read as

$$\frac{1}{v}\frac{\partial \phi(x,t)}{\partial t} = D\nabla^2\phi(x,t) + \Big(\nu\Sigma_f(1-\beta) - \Sigma_a(x,t)\Big)\phi(x,t) + \lambda C(x,t) \tag{51}$$

and

$$\frac{\partial C(x,t)}{\partial t} + u\frac{\partial C(x,t)}{\partial x} = \beta\nu\Sigma_f\phi(x,t) - \lambda C(x,t) \tag{52}$$

with vacuum boundary conditions for the flux, and with

$$C(0,t) = C(H, t-\tau_L)e^{-\lambda\tau_L} \tag{53}$$

for the precursors, where $\tau_L = L / u$. In (51), $\Sigma_a(x,t) = \Sigma_a + \delta\Sigma_a(x,t)$, such that the system is critical with Σ_a. The static and the noise equations, respectively, can be obtained easily from (51) and (52).

Integrating Eq. (52) and substituting into (51) one obtains one single equation for the flux. In the static case it has the form

$$\begin{aligned} &D\nabla^2\phi_0(x) + \Big(\nu\Sigma_f(1-\beta) - \Sigma_a\Big)\phi_0(x) \\ &+e^{-\frac{x\lambda}{u}}\frac{\lambda\beta\nu\Sigma_f}{u}\left[\frac{1}{e^{\lambda\tau}-1}\int_{-a}^{a} e^{\frac{x'\lambda}{u}}\phi_0(x')dx' + \int_{-a}^{x} e^{\frac{\lambda x'}{u}}\phi_0(x')dx'\right] = 0 \end{aligned} \tag{54}$$

It is the streaming term in Eq. (52), likewise the integral terms in Eq. (54), which prevent both a closed form solution and the application of the factorization technique. However, in the case of choosing an infinite fuel circulation velocity, i.e. $u \to \infty$, which can be performed on the integral form, the equations simplify, and a closed analytical solution of both the static and the noise equations can be achieved. This solution is useful in determining the point kinetic component of the noise.

3.4 Derivation of the point kinetic limit in an MSR for infinite fuel velocity

Following Pázsit and Jonsson (2011), for the case of infinite fuel velocity, the static equation, and that of the Green's function of the noise equation, respectively, can be written as

$$\nabla^2\phi_0(x) + B_0^2\phi_0(x) + \frac{\eta_0}{T}\int_{-a}^{a}\phi_0(x')dx' = 0 \tag{55}$$

and

$$\nabla^2 G(x,x_0,\omega) + B^2(\omega)G(x,x_0,\omega) + \frac{\eta(\omega)}{T}\int_{-a}^{a}G(x,x_0,\omega)dx' = \delta(x-x_0) \tag{56}$$

with

$$B^2(\omega) = B_0^2\left(1 - \frac{i\omega\Lambda}{\rho_\infty - \beta}\right),\ \eta(\omega) = \frac{\lambda}{\lambda + i\omega}\frac{\nu\Sigma_f\beta}{D} \tag{57}$$

As described in (Pázsit and Jonsson, 2011), the solution of (55) is given as

$$\phi_0(x) = A[\cos B_0 x - \cos B_0 a] \tag{58}$$

with the criticality condition

$$B_0^2\cos B_0 a + \frac{2a\eta_0}{T}\cos B_0 a - \frac{2\eta_0}{TB_0}\sin B_0 a = 0 \tag{59}$$

The solution for the Green's function reads as

$$G(x,x_0,\omega) = \frac{\eta(\omega)\varphi_0(x,\omega)\varphi_0(x_0,\omega)}{TK(\omega)B^2\cos Ba} - \frac{1}{B\sin 2Ba}\begin{cases}\sin B(a-x_0)\sin B(a+x) & x < x_0\\ \sin B(a+x_0)\sin B(a-x) & x \geq x_0\end{cases} \tag{60}$$

where

$$\varphi_0(x,\omega) = \cos Bx - \cos Ba;\ \ B \equiv B(\omega) \tag{61}$$

has the form of the static flux but with a frequency dependent buckling, and

$$K(\omega) = B^2(\omega)\cos B(\omega)a + \frac{2a\eta(\omega)}{T}\cos B(\omega)a - \frac{2\eta(\omega)}{TB(\omega)}\sin B(\omega)a. \tag{62}$$

From (60) it is seen that for $\omega \to 0$, one has $K(\omega) \to 0$, since (62) reverts to the criticality equation (59). Hence the first term on the r.h.s. of (60) dominates over the second term, which remains finite. The first term, for small ω, has the correct point kinetic form, with the space and frequency dependent terms being factorised, and the space dependent terms having the form of the static flux. Hence, for low frequency, one has

$$G(x,x_0,\omega)^{p.k.} = \frac{\eta(\omega)\phi_0(x)\phi_0(x_0)}{A^2TK(\omega)B^2(\omega)\cos B(\omega)a} \tag{63}$$

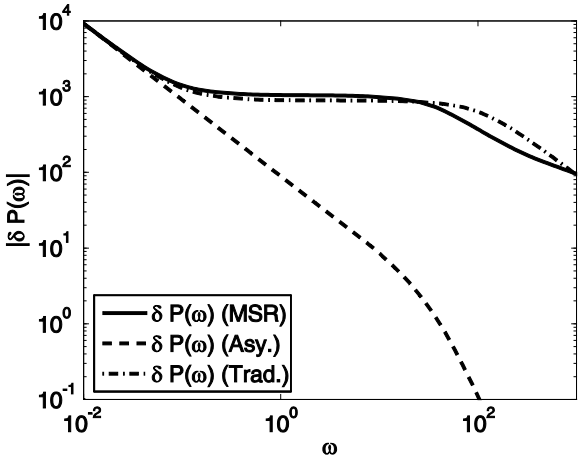

Fig. 30 Comparison of traditional and MSR forms of the frequency dependent part of the point kinetic term.

from which it follows that

$$\delta P^{ASY}(\omega) = G_0(\omega)^{ASY}\rho(\omega) \tag{64}$$

with

$$G_0(\omega)^{ASY} = -\frac{\eta(\omega)\nu\Sigma_f}{TK(\omega)B^2(\omega)\cos B(\omega)a} \tag{65}$$

However, (65) is only valid for low frequencies, where the last term of (60) is negligible besides the first one. The general form of $\delta P(\omega)^{MSR}$ can be obtained by multiplying (55) by $\delta\phi(x,\omega)$, (56) by $\phi_0(x)$, integrating and subtracting the two equations. The result can be given as

$$\delta P(\omega)^{MSR} = \alpha(\omega)\Big[\rho(\omega) + \beta(\omega)\rho\,'(\omega)\Big] \tag{66}$$

where $\alpha(\omega)$ and $\beta(\omega)$ are not given here for brevity, and

$$\rho\,'(\omega) = -\frac{\int_{-a}^{a}\phi_0(x,\omega)\delta\Sigma_a(x,\omega)\phi_0(x)dx}{\nu\Sigma_f\int_{-a}^{a}\phi_0^2(x)dx} \tag{67}$$

This term reverts to the traditional form of the reactivity for small ω where $\phi_0(x,\omega)\approx\phi_0(x)$, but deviates from it for larger ω values. Quantitative results for the various forms of $\delta P(\omega)$ are shown in Fig. 30.

3.5 Conclusions

Calculation of the point kinetic term of the noise is possible in a simplified model of an MSR. The results show that in the general case of arbitrary frequency, the amplitude term cannot be factorised into a product of the traditional reactivity and a zero power transfer function.

4 Development of a simulation model to simulate bubbly two-phase flow with axially dependent void fraction and void velocity

4.1 Introduction

The determination of the void fraction in the core of BWR from in-core neutron noise measurements is not a trivial task and requires some sophisticated techniques to be developed to successfully perform it. Primarily, there are two conceptual methods out of several (both based on the analysis of the thermal neutron noise) which are worth to point out here and thus are discussed thereafter. The first one is based on the strong correlation between the so-called break frequency of the Auto Power Spectral Density (APSD) (Pázsit and Demazière, 2011) of the measured noise and the void content at a corresponding axial core level (Kosály, 1980). Another method refers to the estimation of the transit times for the void fluctuations to propagate between two different detector positions by calculating the Cross Power Spectral Density (CPSD) of the induced neutron noise.

Unfortunately, due to several reasons both methods can not be directly tested on the actual power plant measurements. The difficulty with the first method is related to the fact that the corresponding measured neutron noise is usually filtered and all the frequencies above 16 Hz are suppressed. In practise, the break frequency usually ranges between 10-30 Hz, which makes its proper estimation from the current measurements quite complicated and almost impossible. As for the second method where the vapour velocity is first calculated from averaged void velocity and thereafter the void content is reconstructed, the precise estimation of the transit times is required to provide satisfactory results. An alternative way might be to use the increased number of detector measurements compared to the four ones which are available now.

In order to test both methodologies it is instructive to construct the simple model of a boiling process occurring in a real BWR heated channel (one fuel assembly) and then to simulate the corresponding induced neutron noise. Such a task is the main objective of the present stage. The model is based on the Monte Carlo technique (Pázsit and Glöckler, 1985; Pázsit, 1986; Brown and Sutton, 1996) where the bubbles are generated randomly in both space and time. This approach has already been successfully tested in some earlier neutron noise application such as the modelling of a vibrating control rod or a fuel assembly (Pázsit and Glöckler, 1983, 1984; Pázsit and Demazière, 2011).

The main advantage of this type of model is that, in addition to the simulated neutron noise signals, one has access to the original void and velocity profiles as these constitute model inputs. This provides an exclusive possibility to test the method of determining the void fraction and steam velocity from the neutron noise by comparing two sets of data. Another benefit from using this model is its applicability to the non-stationary processes which is a common assumption in traditional methods.

To this end, the description of the Monte Carlo model is given. The feasibility of the method is demonstrated by displaying the structure (topology) of the generated flow, and some of its characteristic, such the true average void fraction as calculated from the signals with time averaging methods.

4.2 Model construction

In order to set up a realistic model of the two-phase flow using a Monte Carlo technique, a proper distribution for bubble generation should be found. The goal is to construct an equilibrium (stationary) distribution of the void fraction with an axial profile resembling that in an actual BWR void profile. For simplicity, it will be assumed that all bubbles have the same size (diameter), and we shall exclude bubble overlapping (intersection). Under such assumptions, the average void fraction in a sub-volume will be proportional to the density of bubbles. It is easy to see that if the velocity of all bubbles was the same, then, taking also into account the propagation of the already generated bubbles, the bubble generation rate (intensity) per unit length, $p(z)$, which generates a desired void profile $\alpha(z)$, would be proportional to the gradient of the void fraction as

$$p(z) \propto \frac{d\alpha(z)}{dz} \tag{68}$$

However, the velocity of the bubbles will depend on the void fraction, and therefore Eq. (68) will not be valid. The correct formula reads instead as

$$p(z) = v(\alpha(z)) \cdot \frac{d\alpha(z)}{dz} \tag{69}$$

with $v(z) = v(\alpha(z))$ being the axial void velocity. Assuming, for simplicity,

$$v(z) = \frac{v_0}{1-\alpha(z)}, \tag{70}$$

one obtains between the bubble generation profile and the void fraction the relationship

$$p(z) \propto \frac{v_0}{1-\alpha(z)} \cdot \frac{d\alpha(z)}{dz} \tag{71}$$

From Eq. (71), for any given desired void profile $\alpha(z)$, the bubble generation profile $p(z)$ can be determined.

However, since there are no realistic void fraction profiles available in form of simple analytic functions, to keep at least the bubble generation model at a simple level, we will start with choosing a simple form for the bubble generation intensity as being proportional to the static neutron flux as:

$$p(z) = \frac{\pi}{2H} \cdot \sin(\frac{z\pi}{H}), \tag{72}$$

where H denotes the height of the channel. In order to serve as a probability distribution, $p(z)$ is normalized to unity. For the sampling of the bubbles with Monte Carlo methods, one needs to use the cumulative probability function $P(z)$ of the probability distribution $p(z)$ as (Brown and Sutton, 1986)

$$P(z) = \int_0^z p(z')dz', \tag{73}$$

From Eqs. (72) and (73), the cumulative distribution function $P(z)$ is obtained as

$$P(z) = \frac{1}{2}(1 - \cos(\frac{\pi z}{H})) \tag{74}$$

whereby Eq. (74) constitutes the sampling function for the bubble generation in the present Monte Carlo model.

The axial velocity profile of bubbles can be easily estimated from the following steady-state mass conservation equation written for the mixture quantities between the vapour and liquid phases of the coolant:

$$\frac{\partial[\rho_m(z)\cdot v_m(z)]}{\partial z} = 0, \tag{75}$$

where the mixture density and mixture velocity are defined as:

$$\rho_m(z) = \rho_l\cdot(1-\alpha(z)) + \rho_v\cdot\alpha(z), \tag{76}$$

$$v_m(z) = v_l\cdot(1-\alpha(z)) + v_v\cdot\alpha(z), \tag{77}$$

where ρ_l, ρ_v, v_l, v_v are the densities and velocities for the liquid and gaseous phases, respectively. Combining Eqs. (75)-(77), one gets for the axial bubble velocity the result

$$v(z) = v_m(z) = \frac{v_l}{1-\alpha(z) - \frac{\rho_v}{\rho_l}\alpha(z)} \approx \frac{v_0}{1-\alpha(z)}. \tag{78}$$

which was already assumed in (70). Here, $v_0 = v_l$ is the velocity of the liquid phase at the channel inlet. In this model the slip ratio will be taken as unity, such that the void and liquid velocities are assumed to be the same. The third term in the denominator of the last equation is disregarded due to its negligible value. Although Eq. (78) becomes singular when the void fraction reaches unity, it is still applicable to the current Monte Carlo simulation where a void fraction profile is kept close to the real BWR, usually with maximum value below 0.8.

To simplify the simulations, instead of modelling a true 3-D geometry, a two-dimensional model of the heated channel, representing the radial and axial cross-section of a real fuel assembly in (x,z) geometry is chosen. The bubbles are therefore represented as 2-D circles with a fixed diameter. The coordinates of the bubble centres are generated randomly along the x- and z- dimensions. The sampling of the bubbles in the z-direction is performed according to the formula above, whereas, without loss of generality, the sampling in the x-direction is taken as a uniform one. From the conceptual point-of-view, it is important to underline that no overlapping between different bubbles is allowed in the present model.

The bubble diameter is set to $d_{bubble} = 0.8$ cm while the diameter of the heated channel is chosen equal to the typical BWR one $D = 20$ cm. The height of the channel corresponds to the length of a BWR fuel assembly, i.e. to $H = 400$ cm. The bubble inlet velocity is taken to be $v_0 = 200$ cm/s, corresponding to a typical BWR inlet flow velocity under normal operational conditions. To provide proper detector efficiency, the time step in the data processing is selected equal to $\delta t = d_{bubble} / (5v_0) = 0.0008$ seconds, which gives an opportunity to detect the same bubble up to 5 times while it bypasses the detector aperture.

The simulation starts with the generation of 100 bubbles at $t = 0$ s and proceeds with the random injection of 35 new bubbles at each consecutive time step. Since the transient part of the simulation is of no interest here, the recording of calculated void fluctuations is initiated after 60 seconds of the simulation and thus any transient effects

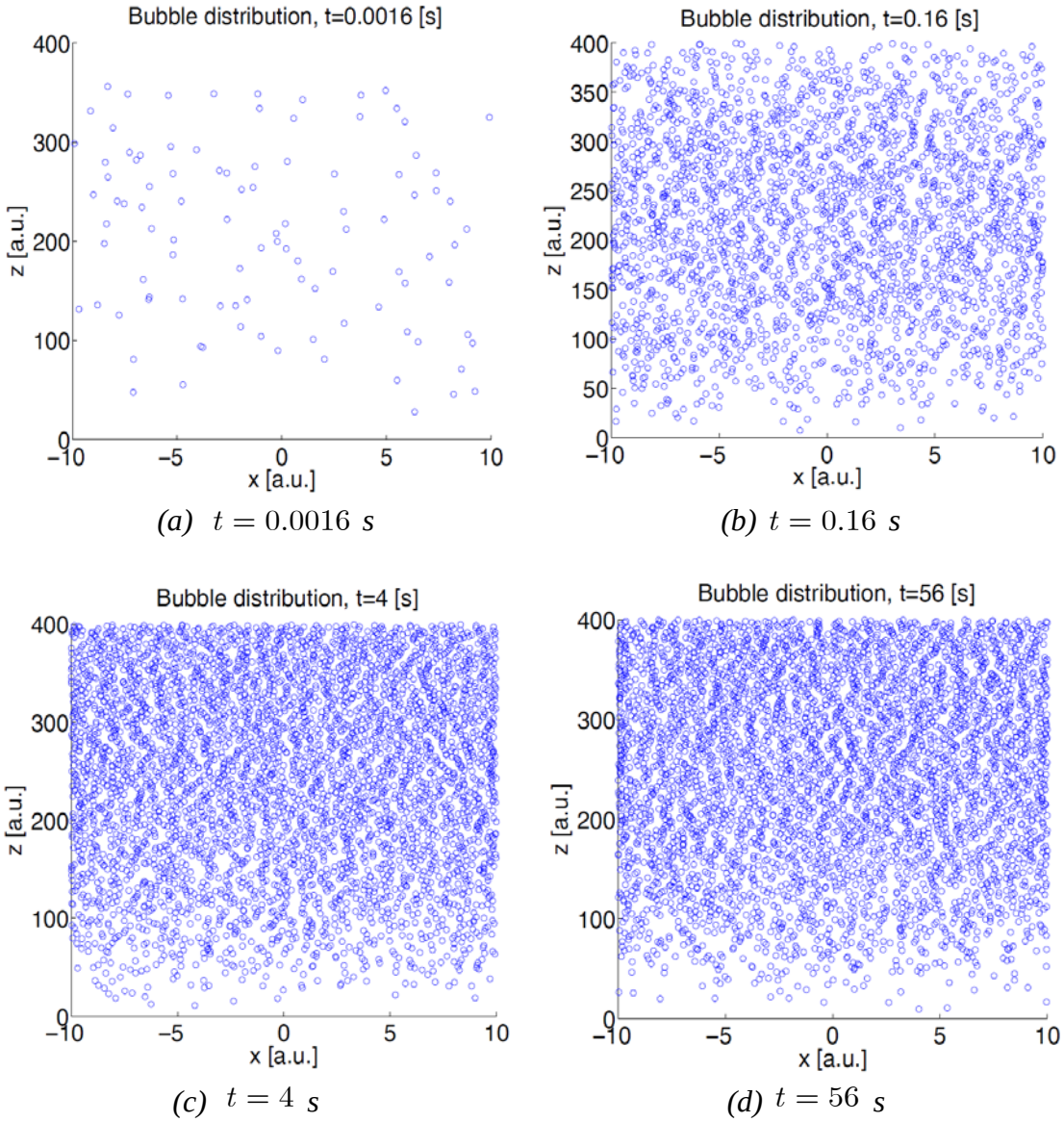

(a) $t = 0.0016$ *s* *(b)* $t = 0.16$ *s*

(c) $t = 4$ *s* *(d)* $t = 56$ *s*

Fig. 31 Illustration of the generated bubbly flow from the Monte Carlo simulations for four different time instants after the start of the bubble generation.

are eliminated. The total simulation time is limited to $T_{sim} = 1320$ seconds. In order to facilitate the void fraction calculations, the entire 2D $x - z$ -plane of the heated channel is divided into horizontal layers, each of the size of $\delta z = 0.1$ cm. The momentary void fraction is then estimated for each axial position between the layers and for each time step by calculating the total intersection length between the bubbles and the corresponding layer boundary. In order to evaluate the void fraction, the total intersection length of bubble crossings for each axial level is weighted with the heated channel diameter D.

An illustration of the simulation results is shown in Fig. 31 for four different times after the start of the simulation. It is seen how the asymptotically stationary flow is formed after a few seconds time. For better visibility, the bubble size is not correct, rather it is enlarged. Hence it looks as if the bubbles overlapped, which is not the case with the true bubble size.

It should be noted here that, for the real application of the model, the void fraction should not exceed the critical value corresponding to the void fraction limit for the bubbly flow regime. The latter means that the bubble generation rate should be properly chosen in order to satisfy the aforementioned condition. However, for better visualization of the methodology, the void fraction in the current model is somewhat higher than the ordinary one for the bubbly flow. Moreover, for the higher void fraction ($\alpha > 0.5$) one cannot consider the bubbles as a fluctuating part inducing the variations in the neutron flux, since both the liquid and vapour parts deviate equally from the mean void fraction.

The axial velocity $v(z)$ is calculated for each axial position separately via Eq. (78). It is worth mentioning that the real bubble velocity is usually a continuous function in space. However, due to discretization, the velocity in the present model is evaluated only in a discrete number of spatial points. Furthermore, due to the random character of bubble production, in particular the instantaneous birth of new bubbles with full diameter, the axial velocity also becomes a random quantity whose momentary values are not

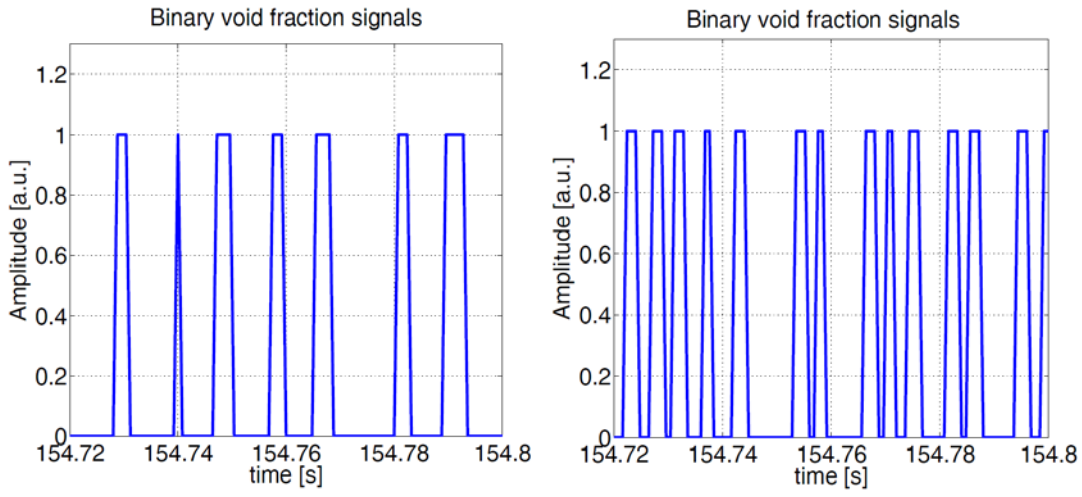

(a) z=60 cm *(b) z=180 cm*

Fig. 32 Binary void fraction signals measured in two axial positions $z = 60$ cm and $z = 180$ cm, respectively.

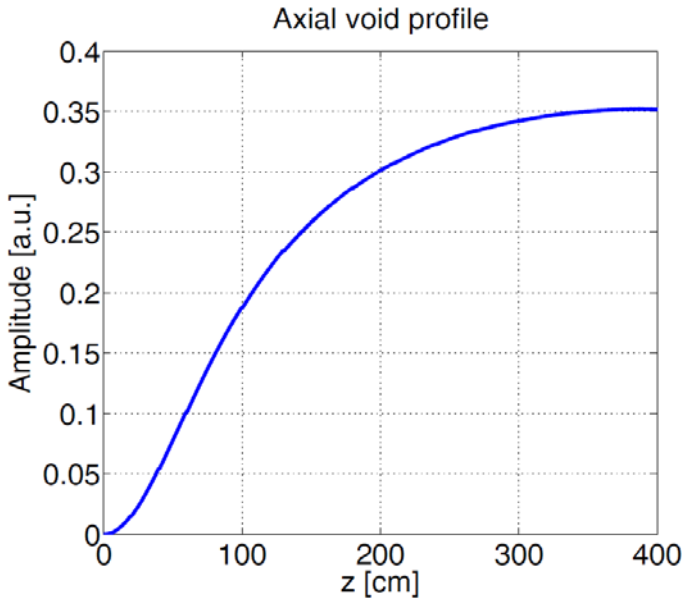

Fig. 33 True axial void profile (the output from Monte Carlo model).

necessarily monotonic as a function of the elevation in the channel. This means that some bubbles having lower axial elevation can move faster than those with a higher axial position, which could lead to bubble intersection, which is undesirable in the present model. To tackle avoid this problem, the velocity profile is re-adjusted from its instantaneous value, which shows some scatter around the smooth axial profile of its mean value, by fitting it to a high order polynomial function. Obviously, in this case the velocity becomes a continuous and monotonic function in space, and no bubble intersection will occur due to bubble transport. From the realisation of the simulation, the final average local void fraction is estimated from the flow itself, by time averaging methods. First, from the simulations, a binary random time signal for the void fraction $\alpha(z,t)$ at any given point z is obtained, whose value equals 1 if the detection point is inside the void, whereas it equals zero if the observation point is in the fluid. Two examples of such simulated signals, corresponding to two different average void fractions, are shown in Fig. 32. Since, when the simulated process reaches the stationary phase, it is also ergodic, the ensemble average $\alpha(z) \equiv \left\langle \alpha(z,t) \right\rangle$ can be estimated by time averaging methods as

$$\alpha(z) = \left\langle \alpha(z,t) \right\rangle = \frac{1}{T} \int_0^T \alpha(z,t) dt$$

Such a void profile is shown in Fig. 33.

4.3 Conclusions

The results shown above indicate that with the random sampling methods of bubble generation and subsequent propagation and adjustment of the velocity of the resulting void-fluid mixture, a sufficiently realistic model of a bubbly two-phase flow was generated for the specified application. The application is to generate synthetic neutron detector signals by convoluting the space-time dependent void fraction fluctuations

$$\delta\alpha(z,t) = \alpha(z,t) - \alpha(z)\,,$$

as a noise source, with a dynamic neutronic transfer function. The various methods of reconstructing the axially dependent average void fraction $\alpha(z)$ from the neutron detector signals, can be tested. This work is nevertheless outside of the present report, and will be included into the research project between Chalmers and Ringhals.

Acknowledgement

This project was supported by the Swedish Nuclear Power Inspectorate, contract No. SSM 2011-2069. Contact person was Assoc. Prof. Ninos Garis.

References

Bell G. and Glasstone S., “Nuclear Reactor Theory”, Van Nostrand Reinhold Company, New York, 1970.

Brown F. B. and Sutton T. M., Monte Carlo fundamentals, The 1996 Frederic Joliot summer school in reactor physics. Modern reactor physics and the modelling of complex systems proceedings, Cadarache & France, August 19-28, pp. 348-352, 1996.

Dam H. van, A perturbation method for analysis of detector response to parametric fluctuations in reactor. *Atomkernenergie* **25**, 70, 1975.

Dam H. van, Neutron noise in boiling water reactors. *Atomkernenergie* **27**, 8, 1976.

Demazière C., Development of a 2-D 2-group neutron noise simulator”. Ann. Nucl. Energy 19, 647 – 680, 2004

Demazière C., CORE SIM: A multi-purpose neutronic tool for research and education. To appear in *Ann. Nucl. Energy,* 2011

Demazière C. and Pázsit I., Power Reactor Noise, Lecture notes, Chalmers University of Technology, Göteborg, 2008.

Demazière C. and Pázsit I., Numerical tools applied to power reactor noise analysis. *Prog. Nucl. Energy* **51**, 67 – 81, 2008

Demazière C., Pázsit I., Sunde C. and Wright J., *Research and Development Program in Reactor Diagnostics and Monitoring with Neutron Noise Methods Stage 10. Final Report*, SKI report 04:57, 2004

Dykin V. Pázsit I., Remark on the role of the driving force in BWR stability. Ann. *nucl. Energy* **36**, pp. 1544 –1552, 2009.

Jonsson A. and Pázsit I. Two-group theory of neutron noise in Molten Salt Reactors. *Ann. nucl. Energy* **38**, 1219-1446, 2011.

Kosály G., “Noise investigations in boiling-water and pressurized-water reactors”, *Progress in Nuclear Energy* **5**, pp. 145-199, 1980.

Pázsit I. and Glöckler O., “On the neutron noise diagnostics of PWR control rod vibrations I. Periodic vibrations”, *Nuclear Science and Engineering*, **Vol. 85**, pp. 167-177, 1983.

Pázsit I. and Glöckler O., “On the neutron noise diagnostics of PWR control rod vibrations II. Stochastic vibrations”, *Nuclear Science and Engineering*, **Vol. 88**, pp. 77-87, 1984.

Pázsit I. and Glöckler O., “Cross sectional identification of two-phase flow by correlation technique”, *Progress in Nuclear Energy*, **Vol. 15**, pp. 661-669, 1985.

Pázsit I., “Two-phase flow identification by correlation techniques”, *Annals of Nuclear Energy*, **Vol. 13**, pp. 37-41, 1986.

Pázsit I., Dynamic transfer function calculations for core diagnostics. Ann. Nucl. Energy 19 (5) 303-312 (1992).

Pázsit I. and Demazière C., "Noise Techniques in Nuclear Systems," in: Handbook of Nuclear Engineering, Vol. 3, Chap. 14, pp 1629-1737, Ed. Dan G. Cacuci, Springer (2010)

Pázsit I. and Garis N. S., *Forskningsprogram angående härddiagnostik med neutronbrusmetoder Etapp I. Slutrapport*, SKI report 95:14, 1995.

Pázsit I., Garis N. S. and Thomson O., *Forskningsprogram angående härddiagnostik med neutronbrusmetoder Etapp 2. Slutrapport*, SKI report 96:50, 1996.

Pázsit I., Garis N. S., Karlsson J. and Rácz A., *Forskningsprogram angående härddiagnostik med neutronbrusmetoder Etapp 3. Slutrapport*, SKI report 97:31, 1997

Pázsit I. and Karlsson J K-H, *Research and Development Program in Reactor Diagnostics and Monitoring with Neutron Noise Methods Stage 4. Final report.*, SKI report 98:25, 1998

Pázsit I., Karlsson J K-H, Lindén P. and Arjanov V., *Research and Development Program in Reactor Diagnostics and Monitoring with Neutron Noise Methods Stage 5. Final report*, 1999

Pázsit I., Demazière C., Avdic S. and Dahl B., *Research and Development Program in Reactor Diagnostics and Monitoring with Neutron Noise Methods Stage 6. Final Report*, SKI report 00:28, 2000

Pázsit I., Demazière C., Arzhanov V. and Garis N. S., *Research and Development Program in Reactor Diagnostics and Monitoring with Neutron Noise Methods Stage 7. Final Report*, SKI report 01:27, 2001

Pázsit I., Demazière C. and Arzhanov V., *Research and Development Program in Reactor Diagnostics and Monitoring with Neutron Noise Methods Stage 8. Final report*, SKI report 03:08, 2003a

Pázsit I., Arzhanov V., Nordlund A. and Olsson D., *Research and Development Program in Reactor Diagnostics and Monitoring with Neutron Noise Methods Stage 9. Final Report*, SKI report 03:30, 2003b

Pázsit I., C. Demazière, C. Sunde, P. Bernitt and A. Hernández-Solís (2008), *Final Report on the Research Project Ringhals Diagnostics and Monitoring, Stage 12*. CTH-NT-220/RR-14, August 2008, Chalmers University of Technology, Sweden

Pázsit I., Wihlstrand G., Tambouratzis T. and Dahl B., *Research and Development Program in Reactor Diagnostics and Monitoring with Neutron Noise Methods, Stage 13*, SSM report 2008:39, 2009

Pázsit I., Wihlstrand G., Tambouratzis T., Jonsson A. and Dahl B., *Research and Development Program in Reactor Diagnostics and Monitoring with Neutron Noise Methods, Stages 14 and 15*, SSM report 2009:38, 2009.

Pázsit I., Dykin V., Jonsson A. and Demazière C., *Research and Development Program in Reactor Diagnostics and Monitoring with Neutron Noise Methods, Stage 16*, SSM report 2010:22, 2010

Pázsit I., Tran H. N., Dykin V. and Jonsson A., *Research and Development Program in Reactor Diagnostics and Monitoring with Neutron Noise Methods, Stage 17*, SSM report 2011:29, 2011

Pázsit I., C. Montalvo Martín, V. Dykin and T. Tambouratzis (2010), *Final Report on the Research Project Ringhals Diagnostics and Monitoring, Stage 13*. CTH-NT-230/RR-15, March 2010, Chalmers University of Technology, Sweden, 2010

Pázsit I., C. Montalvo-Martin, A. Hernandez-Solis, P. Bernitt Cartemo, Diagnostics of core barrel and fuel assembly vibrations in the Ringhals PWRs, Sweden, Proc. NPIC&HMIT 2010, Las Vegas, Nevada, Nov. 7 2010, American Nuclear Society, LaGrange Park, IL.

Pázsit I., Dykin V., Investigation of the space-dependent noise induced by propagating perturbations. *Ann. nucl. Energy* **37**, pp. 217 –2376, 2010.

Pázsit I. and Jonsson A., Reactor kinetics, dynamic response and neutron noise in Molten Salt Reactors (MSR). *Nucl Sci. Engng* **167**, 61 – 76, 2011

SIMULATE-3: Advanced Three-Dimensional Two-Group Reactor Analysis Code, The User's Manual for SIMULATE-3, *Studsvik Scandpower Inc.*, USA, 2001.

Sunde C., Pázsit I., Demazière C., Dahl B. and Mileshina L., *Research and Development Program in Reactor Diagnostics and Monitoring with Neutron Noise Methods Stage 11 and 12. Final report*, SKI report 2006:34, 2006

Sunde C., Demazière C., and Pázsit I., Final report on the Research Project Ringhals Diagnostics and Monitoring, Stage 11. Chalmers internal report CTH-NT-206/RR13, Chalmers University of Technology, Sweden (2007).

Sweeney F. J., J. March-Leuba and C. M. Smith, “Contributions of fuel vibrations to ex-core neutron noise during the first and second fuel cycles of the Sequoyah-1 pressurized water reactor”. Prog. Nucl. Energy Vol. 15, pp 283-290, 1985

Williams M. M. R., “Random Processes in Nuclear Reactors”, Pergamon Press, Oxford, New York, Tokyo, 1974.

Yoshioka H., Pázsit I., Otake H. and Nishina K., “Analysis of temporal and spatial decay of pulsed neutrons in single- and multiple-core systems”, *Annals of Nuclear Energy* **25**, pp. 1169 – 1193, 1998.

2013:04

The Swedish Radiation Safety Authority has a comprehensive responsibility to ensure that society is safe from the effects of radiation. The Authority works to achieve radiation safety in a number of areas: nuclear power, medical care as well as commercial products and services. The Authority also works to achieve protection from natural radiation and to increase the level of radiation safety internationally.

The Swedish Radiation Safety Authority works proactively and preventively to protect people and the environment from the harmful effects of radiation, now and in the future. The Authority issues regulations and supervises compliance, while also supporting research, providing training and information, and issuing advice. Often, activities involving radiation require licences issued by the Authority. The Swedish Radiation Safety Authority maintains emergency preparedness around the clock with the aim of limiting the aftermath of radiation accidents and the unintentional spreading of radioactive substances. The Authority participates in international co-operation in order to promote radiation safety and finances projects aiming to raise the level of radiation safety in certain Eastern European countries.

The Authority reports to the Ministry of the Environment and has around 270 employees with competencies in the fields of engineering, natural and behavioural sciences, law, economics and communications. We have received quality, environmental and working environment certification.

Strålsäkerhetsmyndigheten
Swedish Radiation Safety Authority

SE-171 16 Stockholm
Solna strandväg 96

Tel: +46 8 799 40 00
Fax: +46 8 799 40 10

E-mail: registrator@ssm.se
Web: stralsakerhetsmyndigheten.se